Title

Fluorescence Correlation Spectroscopy Reveals Efficient Cytosolic Delivery of Protein Cargo by Cell-Permeant Miniature Proteins

Journal

ACS Central Science, 4(10)

ISSN

2374-7943

Authors

Wissner, Rebecca F
Steinauer, Angela
Knox, Susan L
et al.

Publication Date

2018-10-24

DOI

10.1021/acscentsci.8b00446

Peer reviewed

ACS central science

Research Article

Cite This: ACS Cent. Sci. 2018, 4, 1379−1393

http://pubs.acs.org/journal/acscii

Fluorescence Correlation Spectroscopy Reveals Efficient Cytosolic Delivery of Protein Cargo by Cell-Permeant Miniature Proteins

Rebecca F. Wissner,[†] Angela Steinauer,[†] Susan L. Knox,[†] Alexander D. Thompson,[†] and Alanna Schepartz*[,†,§]

[†]Department of Chemistry, and [§]Department of Molecular, Cellular, and Developmental Biology, Yale University, New Haven, Connecticut 06520-8107, United States

Supporting Information

ABSTRACT: New methods for delivering proteins into the cytosol of mammalian cells are being reported at a rapid pace. Differentiating between these methods in a quantitative manner is difficult, however, as most assays for evaluating cytosolic protein delivery are qualitative and indirect and thus often misleading. Here we make use of fluorescence correlation spectroscopy (FCS) to determine with precision and accuracy the relative efficiencies with which seven different previously reported "cell-penetrating peptides" (CPPs) transport a model protein cargo—the self-labeling enzyme SNAP-tag—beyond endosomal membranes and into the cytosol. Using FCS, we discovered that the miniature protein ZF5.3 is an exceptional vehicle for delivering SNAP-tag to the cytosol. When delivered by ZF5.3, SNAP-tag can achieve a cytosolic concentration as high as 250 nM, generally at least 2-fold and as much as 6-fold higher than any other CPP evaluated. Additionally, we show that ZF5.3 can be fused to a second enzyme cargo—the engineered peroxidase APEX2—and reliably delivers the active enzyme to the cell interior. As FCS allows one to realistically assess the relative merits of protein transduction domains, we anticipate that it will greatly accelerate the identification, evaluation, and optimization of strategies to deliver large, intact proteins to intracellular locales.

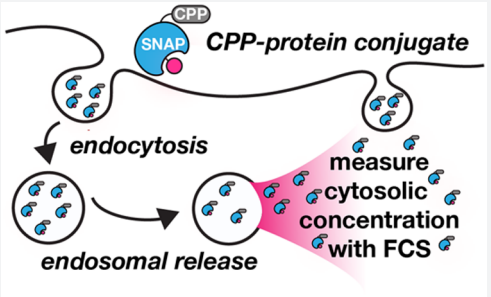

INTRODUCTION

The approval of recombinant human insulin in 1982 heralded the emergence of protein-based therapeutics as a major pharmaceutical class.[1,2] As of late 2017, 239 therapeutic proteins and peptides (also known as biologics) have been approved for clinical use in the U.S.[1] This class encompasses hormones, coagulation factors, and monoclonal antibodies that act in plasma or on the cell surface[2] to combat cancer,[3,4] diabetes,[5] autoimmune disorders,[6−9] hematological disorders,[10] lysosomal storage disorders,[11,12] and other human diseases.[2] Despite this progress, the potential of protein-based therapeutics remains grossly underdeveloped—not a single FDA-approved biologic acts on a molecular target within the cytosol or nucleus. The extreme challenge of delivering intact proteins to the cell interior hampers the use of these materials as potential therapeutics and research tools.

Hundreds of putative cell-penetrating peptides (CPPs) have been studied in the hope of overcoming the challenges associated with intracellular protein delivery.[13] The most common CPPs contain multiple arginine and/or lysine residues, bear a high net positive charge, and exhibit some structural disorder.[14] These unstructured CPPs (uCPPs), a class that includes Tat_{48-60},[15] penetratin,[16] oligo-arginine sequences,[17,18] and others,[19] have been reported to deliver assorted protein, nucleic acid, small molecule, and nanoparticle cargoes with varying success.[20] Numerous studies have confirmed that at low micromolar concentrations, most (although not all)[21] uCPP−protein conjugates enter cells via energy-dependent endocytic mechanisms.[22−25] However, trafficking to the cytosol requires at least two steps: uptake from the cell surface into the endocytic pathway and release from endosomes into the cytosol. The problem is that although uptake of uCPP−cargo conjugates into endosomes can be efficient, their subsequent release into the cytosol is not.[26] As a result, most uCPP−cargo conjugates are destined for lysosomes and ultimately degraded.[27] Despite this inherent limitation, several uCPP-derived therapeutics have yielded promising results for a variety of disease models, suggesting that even very low delivery levels can establish a therapeutic effect in some cases.[28] Our group and many others have focused on the development of improved strategies to promote endosomal release and thereby facilitate the delivery of peptides and proteins into the cytosol.[29−45]

A critical challenge limiting the development of truly cell-permeant peptides and proteins is the absence of convenient and direct assays to determine the concentration of intact cargo that reaches the cytosol or nucleus. Most assays used for this purpose are qualitative, indirect, or amplify a small signal in a nonlinear manner. The most common qualitative assay evaluates cells treated with a fluorescently labeled CPP−cargo conjugate using both flow cytometry and confocal microscopy.

Received: July 9, 2018
Published: September 27, 2018

DOI: 10.1021/acscentsci.8b00446
ACS Cent. Sci. 2018, 4, 1379−1393

As pointed out previously,[38,46,47] although flow cytometry and confocal microscopy provide qualitative information about total cellular uptake, neither distinguishes fluorescent material in the cytosol or nucleus from that adhered to the plasma membrane or trapped within endosomal (or other) compartments. Microscopy-based experiments can be especially misleading because even mild fixation leads to the intracellular redistribution of CPPs from endosomes to the cytosol. Additionally, membrane-associated peptides, if not carefully removed using trypsin, can contribute to the fluorescence signal intensity observed by microscopy or flow cytometry.[23]

As an alternative to flow cytometry and confocal microscopy, several groups have reported functional or fluorescence-based assays to evaluate cytosolic localization. Functional assays include those based on the recombination and expression of a reporter gene mediated by Cre recombinase[36,48−50] or Cas9;[49] although these assays are easy to implement, they can also be misleading because the relationship between delivery and assay read-out is amplified, not linear. Other qualitative functional assays are based on the cytosolic delivery of small molecule-tagged peptides that illicit a measurable phenotypic change, such as luciferin-tagged peptides reacting with cytosolic luciferase to produce a luminescent read-out,[51] or dexamethasone-tagged peptides for inducing the glucocorticoid-mediated translocation of cytosolic eGFP into the nucleus. These assays are also easy to implement, but often assume that the luciferase−luciferin (or dexamethasone−GR) interaction is unaffected by the cargo. Alternatively, protein fusions that can only be enzymatically modified in cell cytosol, such as ubiquitin[37,52] or avi-tagged protein variants[53,54] (substrates of cytosolic deubiquitinases and biotin ligase, respectively) have been used as model cargos for assessing cytosolic delivery. However, this approach requires the addition of a small protein or large peptide tag to the cargo under study, which may not always be tolerated in a protein sequence. Moreover, both methods require analysis by Western blot, which is not reliably quantitative.[55] Fluorescence-based assays for evaluating delivery into the cytosol include FRET-based systems,[56] fluorogenic probes that turn on in the presence of cell cytosol[57] or cytosolic enzymes,[58,59] and split GFP reporter assays.[30,60,61] However, in all cases these methods yield an amplified or indirect read-out that is only appropriate for rendering qualitative or semiquantitative comparisons of cytosolic delivery. Recently, Peraro et al. developed a high-throughput cell penetration assay based on the Halo-tag system.[62] While this assay quantitatively compares the cytosolic levels achieved by chloroalkane-tagged peptides, it is unable to distinguish degraded material from that which reaches the cytosol intact. Moreover, it has not yet been adapted for assessing the delivery of large proteins into cell cytosol. Taken together, the lack of a reliable method for directly measuring the cytosolic concentrations achieved by cell-permeant peptides and proteins has hindered progress in the field for years.

We have previously reported that small, folded miniature proteins derived from avian pancreatic polypeptide (aPP) or an isolated zinc-finger (ZF) domain can be rationally engineered for high cell uptake,[38,46,63] and that their trafficking to the cytosol can be determined with accuracy and precision using fluorescence correlation spectroscopy (FCS).[47] FCS is a powerful single-molecule technique capable of measuring the concentration of a fluorescent molecule in the cytosol or nucleus of a live cell.[64,65] During an FCS experiment, one records the time-dependent fluctuations in fluorescence intensity of single fluorescent molecules passing through a small (sub-femtoliter) focal volume. These time-dependent fluctuations can be autocorrelated to extract meaningful physical parameters such as the diffusion coefficient and local concentration of the fluorescent molecule.[66] Using FCS, we found that miniature proteins containing a discrete array of five α-helical arginine side chains reached the cytosol in exceptional yields with transport efficiencies ranging from 50−75%.[47] Notably, the transport efficiency of the most efficient cell-permeant miniature protein (CPMP) ZF5.3 exceeded by nearly 10-fold the values measured for previously reported uCPPs.

Intrigued by the efficiencies with which the isolated CPMPs aPP5.3 and ZF5.3 traffic into the cytosol, we sought to evaluate their ability to deliver large proteins into cells in a direct, head-to-head comparison with several other peptide-based delivery vehicles. Specifically, we made use of a commercial, easy-to-use FCS system to directly quantify the relative efficiencies with which two traditional uCPPs, three CPMPs, and two recently reported cell-penetrating cyclic peptides (cCPPs) deliver a full-length protein cargo—the self-labeling enzyme SNAP-tag[67]—into the cytosol of mammalian cells. Using FCS and this set of fluorescent SNAP-tag conjugates (Figure 1A), we discovered that the CPMP ZF5.3 remains a superior cytosolic delivery vehicle even when appended to an enzyme cargo of significant mass. When delivered by ZF5.3, SNAP-tag can achieve a cytosolic concentration as high as 250 nM, generally at least 2-fold and as much as 6-fold higher than any other CPP

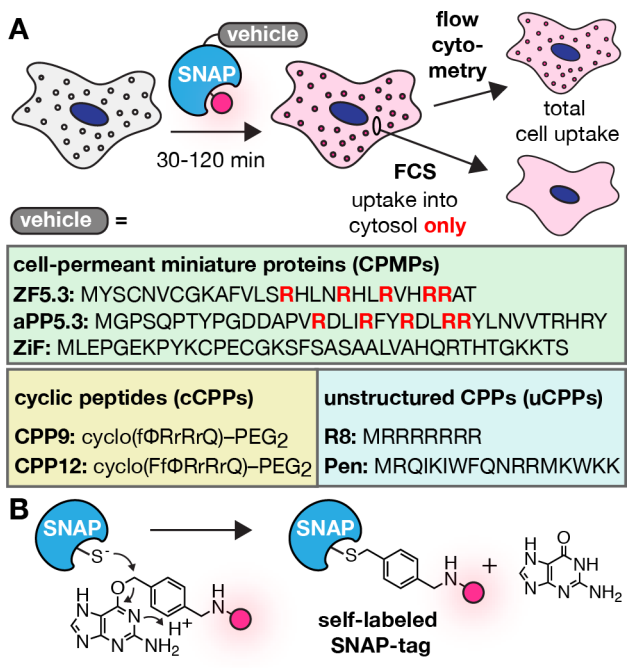

Figure 1. (A) Workflow to determine the overall uptake and cytosolic concentration of a self-labeled CPMP, cCPP, or uCPP SNAP-tag conjugate using flow cytometry and FCS. The sequence of each vehicle studied in this report is listed above. For ZF5.3 and aPP5.3, the residues comprising the 5.3 motif are shown in red. For CPP9 and CPP12, lowercase letters represent D-amino acids, Φ represents L-naphthylalanine, and PEG2 represents a 2-unit ethylene glycol spacer. (B) Mechanism of SNAP-tag self-labeling with a fluorophore-containing benzylguanine derivative.

DOI: 10.1021/acscentsci.8b00446
ACS Cent. Sci. 2018, 4, 1379−1393

evaluated. As we have reported previously, the extent of cytosolic localization does not always mirror the extent of overall uptake ascertained by flow cytometry, demonstrating the value of a technique that measures concentration directly, such as FCS. To demonstrate that ZF5.3-mediated delivery is not restricted to a single protein, we conjugated it to the enzyme APEX2,[68] assessed cytosolic trafficking using FCS, and evaluated peroxidase activity *in cellulo*. Taken together, we have shown that FCS can realistically assess the relative merits of protein transduction domains for shuttling protein cargo beyond membrane barriers, and that the CPMP ZF5.3 holds particular promise as a robust tool for delivering active enzymes into cells.

RESULTS AND DISCUSSION

The Self-Labeling Protein SNAP-tag as a Common, Easily Labeled Cargo. In order to provide a direct and quantitative comparison of protein delivery by previously reported uCPPs, CPMPs, and cCPPs, we sought a well-characterized protein that could be labeled in a homogeneous and stoichiometric manner with a bright photostable dye. We envisioned that this goal would be achieved most easily using a well-studied, self-labeling protein tag such as SNAP,[67] CLIP,[69] or Halo.[70] While we considered using FCS-compatible red fluorescent proteins as model cargo, we were concerned by their complex photophysical properties and known tendency to form multimers *in vitro* and in live cells.[71,72] By contrast, SNAP-tag, an engineered human O^6-alkylguanine-DNA-alkyltransferase variant, reacts efficiently, *in vitro* and *in vivo*, with fluorophore-substituted O^6-benzylguanine (BG) or chloropyrimidine (CP) substrates to form covalent SNAP-tag-fluorophore conjugates (Figure 1B). Virtually all SNAP-tag-protein fusions retain O^6-alkylguanine-DNA-alkyltransferase activity and the ability to self-label.[73] Moreover, the SNAP-tag enzyme is monomeric, highly thermostable (T_M = ~70 °C), and resists degradation by intracellular proteases ($t_{1/2}$ = ~42 h in HEK293T cells).[74] These features render SNAP-tag an attractive model enzyme for the comparative evaluation of uCPP, CPMP, and cCPP-mediated cytosolic delivery.

Previously, we reported FCS experiments that measured the cytosolic concentrations attained when the isolated CPMPs aPP5.3 and ZF5.3 were incubated with cells in culture, but we did not evaluate their ability to deliver appended protein cargo. In this work, we chose to compare cargo delivery by aPP5.3 and ZF5.3 to three canonical uCPPs—R8, Tat, and penetratin (Pen, also known as antennapedia)—and to the zinc finger known as ZiF.[13,20,37] The materials needed for this comparison were easy to prepare, as each CPMP or uCPP is genetically encodable. Indeed, the C-terminally His-tagged SNAP-tag fusion proteins ZF5.3-SNAP, aPP5.3-SNAP, ZiF-SNAP, R8-SNAP, and Pen-SNAP, as well as the control protein SNAP lacking an appended CPP, expressed readily in *Escherichia coli* and were purified to homogeneity by immobilized metal affinity chromatography (IMAC). Notably, the isolated yields of the CPMP-SNAP conjugates ZF5.3-SNAP, aPP5.3-SNAP, and ZiF-SNAP were much higher (20−30 mg/L) than those of the uCPP-SNAP conjugates R8-SNAP and Pen-SNAP (5 mg/L). Following purification, the identity of each protein was confirmed by mass spectrometry (MS), and the purity was assessed by SDS-PAGE (Figure S1). We were unfortunately unable to isolate any full-length Tat-SNAP even after significant experimental optimization, and no additional experiments were performed with this conjugate.

We also sought to compare aPP5.3 and ZF5.3 to a set of cyclic peptides that have been reported by others to enter the cell cytosol, most notably CPP9 and CPP12, sequence variants of the cyclic peptide known as cFΦR4.[35,76] In previous work, cytosolic localization of the isolated CPP9 and CPP12 peptides (no cargo) was estimated from flow cytometry experiments using variants linked covalently to a dye that is ~10-fold more fluorescent at neutral pH than at pH ≤ 6.0; like other assays based on fluorescence intensity, this method provides only an estimate of cytosolic concentration.[57,76] Using this assay, the cytosolic trafficking of CPP9 and CPP12 was estimated to approach that of aPP5.3, which encouraged us to evaluate their relative merits using the more quantitative method of FCS and in a more relevant context in which both are linked to a model cargo protein.[76] However, unlike the uCPPs and CPMPs described above, CPP9 and CPP12 contain nonproteinogenic amino acids and cannot be easily genetically encoded to produce the requisite fusion protein. In an earlier study, cFΦR4 was conjugated to the *N*-terminus of a protein using the peptide carrier protein Sfp phosphopantetheinyl transferase (Sfp).[35] While this method allows for site-specific labeling, it requires modification of the protein of interest with an 11-residue Sfp recognition sequence.[77] Moreover, Sfp labeling requires CoA-derivatized peptides, which require multiple steps after solid phase synthesis to prepare and are costly to scale.[35] Rabideau et al. have shown that the enzyme sortase can ligate unnatural synthetic peptides, including cyclic peptides, onto the C-terminus of full-length proteins.[78] Inspired by this report, we designed a straightforward strategy to ligate CPP9 and CPP12 to the *N*-terminus of SNAP-tag through a covalent linkage (Figure 2). The identity and purity of each cCPP-

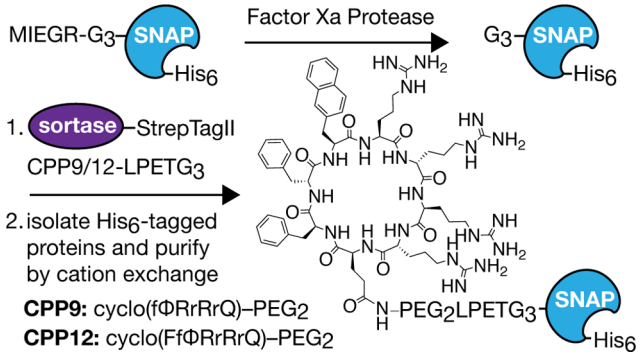

Figure 2. Sortase-based ligation strategy for generating CPP9- and CPP12-SNAP. To prepare SNAP-His_6 bearing an *N*-terminal triglycine sequence for sortase labeling, we expressed and purified a variant containing an *N*-terminal Factor Xa recognition site (MIEGR) followed by a triglycine motif to yield MIEGR-G_3-SNAP-His_6. MIEGR-G_3-SNAP-His_6 was cleaved with Factor Xa to yield G_3-SNAP-His_6. G_3-SNAP-His_6 was then incubated with excess CPP9-$LPETG_3$ or CPP12-$LPETG_3$ in the presence of the engineered sortase variant SrtA7M[75] to generate the desired conjugate in good (>50%) yields. To isolate CPP9- and CPP12-SNAP-His_6 from the reaction mixture, we employed a two-step chromatographic strategy to isolate the desired conjugates (see Methods for additional details).

SNAP-tag conjugate were ultimately assessed by MS and SDS-PAGE, respectively (Figure S1). To prepare for FCS, each SNAP-tag conjugate was incubated with BG-Lissamine rhodamine B (Rho) for 2 h at 37 °C. Rho was selected as the dye of choice because it is compatibile with FCS and cannot penetrate cells on its own.[47] All of the SNAP-tag conjugates

DOI: 10.1021/acscentsci.8b00446
ACS Cent. Sci. 2018, 4, 1379−1393

that we examined retained robust self-labeling activity *in vitro*; in each case, we observed quantitative and homogeneous labeling. SDS-PAGE and MS analyses confirmed the identity, homogeneity, and purity of each Rho-labeled SNAP-tag conjugate used in cellular assays (Figure S2).

Comparing Overall Uptake: Confocal Microscopy. With a set of fluorescently tagged SNAP-tag conjugates in hand, we first sought to evaluate their overall uptake into cells using confocal microscopy (Figure 3). Saos-2 cells were incubated for 30 min with 1 μM of each Rho-labeled SNAP-tag conjugate and then with 300 nM Hoechst 33342 to visualize the cell nucleus. The cells were washed, treated with trypsin to remove surface-bound protein and lift the cells, replated onto fibronectin-coated glass microscopy slides, and imaged. These images (Figure 3A) revealed low levels of intracellular fluorescence when cells were treated with SNAP-Rho and CPP9-SNAP-Rho, suggesting that under these conditions, the presence of CPP9 does not significantly enhance the uptake of an appended SNAP-tag cargo by Saos-2 cells. Cells treated with CPP12-SNAP-Rho, aPP5.3-SNAP-Rho, R8-SNAP-Rho, ZiF-SNAP-Rho, and Pen-SNAP-Rho exhibited bright punctate fluorescence, suggesting significant levels of endocytic uptake, but no observable cytosolic fluorescence. Saos-2 cells treated with ZF5.3-SNAP-Rho displayed bright punctate fluorescence as well as diffuse cytosolic fluorescence, suggesting significant levels of both endocytic uptake and cytosolic release. Overall, these qualitative confocal microscopy results suggest that ZF5.3-SNAP-Rho reaches the cytosol of Saos-2 cells, whereas the other conjugates do so to a lesser extent or not at all.

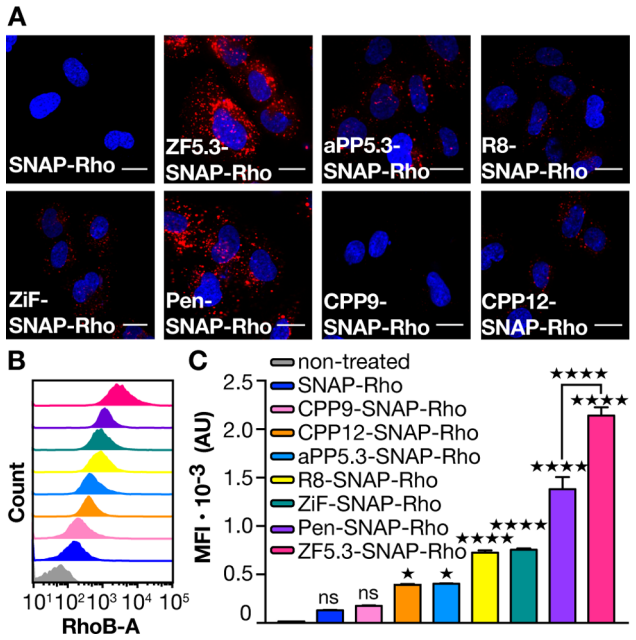

Figure 3. Total cell uptake of Rho-tagged SNAP-tag conjugates assessed by confocal microscopy (A) and flow cytometry (B and C). (A) Images of live Saos-2 cells treated with 1 μM of each SNAP-tag conjugate for 30 min. Scale bar = 20 μm. (B) Histograms and (C) bar plots illustrating the relative uptake of each Rho-tagged SNAP-tag conjugate after 30 min incubation and trypsin treatment to remove surface bound protein. MFI values represent the average median fluorescence intensity of cells determined from 4−12 individual replicates (10 000 cells each). Error bars represent the standard error of the mean. MFI values corresponding to each SNAP-tag conjugate were statistically compared to nontreated cells. ****$p \leq 0.0001$, ***$p \leq 0.001$, **$p \leq 0.01$, *$p \leq 0.05$; one-way ANOVA followed by post hoc Dunnett's test.

Quantifying Overall Uptake: Flow Cytometry. The differences in the overall uptake of each SNAP-tag conjugate suggested by confocal microscopy were studied further using flow cytometry. Treatment of Saos-2 cells with 1 μM of each Rho-labeled SNAP-tag conjugate as described above led to evenly distributed populations of fluorescent cells (Figure 3B); the median fluorescence intensity of this distribution over 3−5 independent replicates is also shown (Figure 3C). Overall, the CPPs and CPMPs studied fall into four categories: cells treated with CPP9-SNAP-Rho were not measurably more fluorescent than cells treated with SNAP-Rho, as expected from the microscopy experiments described above. Cells treated with CPP12-SNAP-Rho and aPP5.3-SNAP-Rho showed comparable levels of fluorescence throughout the cell interior, reaching values approximately 2-fold higher than that observed when cells were treated with SNAP-Rho. Cells treated with R8-SNAP-Rho and ZiF-SNAP-Rho exhibited higher levels of total cellular fluorescence that were nearly 5-fold higher than that of cells treated with SNAP-Rho. The highest levels of total intracellular fluorescence were observed when cells were treated with Pen-SNAP-Rho (an 11-fold increase relative to cells treated with SNAP-Rho) and ZF5.3-SNAP-Rho (a 17-fold increase relative to cells treated with SNAP-Rho). Overall, we observed good agreement between data from confocal microscopy and flow cytometry experiments performed using Saos-2 cells.

To broaden these findings, we repeated the flow cytometry experiments in two other common cell lines (HeLa and SK-HEP-1) and obtained similar results, implying that the level to which each SNAP-tag conjugate is taken up by endocytosis is comparable within this set of cell lines (Figure S3). These results are consistent with previous flow cytometry studies demonstrating that the overall cellular uptake of ZF5.3 is significantly higher than that of uCPPs and other CPMPs.[46,47] Our results are also consistent with flow cytometry studies demonstrating that the total levels of ZiF-mediated protein delivery are similar to those achieved by uCPPs.[37] In addition, we found the overall uptake of Pen-SNAP-Rho to be significantly higher than that of R8-SNAP-Rho, which contradicts several uptake studies performed with molecules lacking an appended cargo.[25,79,80] Finally, in light of a previously published report,[76] we were surprised to find that the overall uptake of cCPP-SNAP-tag conjugates (CPP9-SNAP-Rho and CPP12-SNAP-His$_6$-Rho) were significantly lower than those measured for any other tested uCPP or CPMP conjugate. As a whole, our results demonstrate that the CPMP ZF5.3 promotes the efficient uptake of a large appended protein cargo across multiple cell lines, while other CPMPs, uCPPs, and cCPPs do so to a lesser extent.

Quantifying Cytosolic Localization: Fluorescence Correlation Spectroscopy (FCS). After assessing cellular uptake by confocal microscopy and flow cytometry, we used FCS to determine the amount of labeled SNAP-tag protein that reaches the cytosol of live cells. Saos-2 cells were prepared for FCS experiments in the same manner as described for confocal microscopy. After confocal images were acquired, cells were scanned visually to identify locations for cytosolic focal volume placement; nuclear regions were avoided, as were regions with high punctate signal representative of endosomes. The acquired correlation data were fit to a three-dimensional (3D) diffusion model containing a parameter for anomalous

DOI: 10.1021/acscentsci.8b00446
ACS Cent. Sci. 2018, 4, 1379−1393

subdiffusion using a custom MATLAB script as previously described.[47] The average diffusion times (τ_D) of the SNAP-tag conjugates (Figure 4A) measured in the cytosol ranged between 1.20 ± 0.66 and 2.67 ± 0.37 ms, approximately 6−14-fold higher than values acquired *in vitro* (Figure S4), in good agreement with the observed increase in cytoplasmic diffusion times observed for intact peptides/proteins in living cells.[47,81] Notably, the intracellular diffusion time of each SNAP-tag conjugate is at least 5-fold longer than the average intracellular diffusion time measured for the 3.4 kDa Rho-tagged stable peptide ZF5.3^R (0.21 ± 0.025 ms).[47] Since diffusion time is proportional to molecular mass, this difference provides strong evidence that the detected fluorescent signals represent dye-protein conjugates and not released dye or small protein fragments. To confirm that SNAP-tag remains intact once delivered to the cytosol, cytosolic fractions obtained from nontreated cells and from cells treated with ZF5.3-SNAP-Rho were loaded onto an SDS-PAGE gel and analyzed by in-gel fluorescence scanning followed by Western blotting with an anti-SNAP-tag antibody. The cytosolic fraction obtained from cells treated with ZF5.3-SNAP-Rho contained a single fluorescent band that was positively identified as SNAP-tag by Western blot analysis (Figure S5).

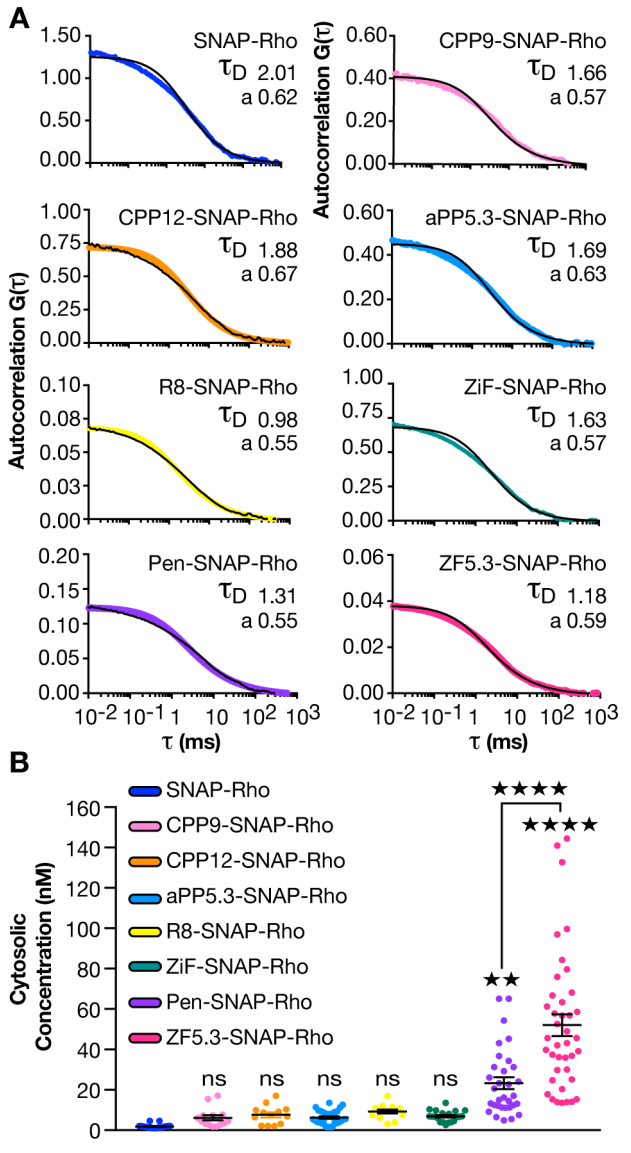

Figure 4. Quantification of cytosolic delivery of Rho-tagged SNAP-tag conjugates using FCS. Saos-2 cells were treated with 1 μM of each SNAP-tag conjugate for 30 min and replated for FCS in the same manner as described for confocal microscopy in Figure 2. (A) Representative *in cellulo* FCS traces corresponding to each indicated Rho-tagged SNAP-tag conjugate displaying the measured diffusion time (τ_D) as well as the anomalous coefficient (a) associated with each representative trace. (B) Scatter plot representation of intracellular concentrations of Rho-tagged SNAP-tag conjugates determined from respective autocorrelation fits. The average cytosolic concentrations corresponding to each Rho-tagged SNAP-tag conjugate were statistically compared to the intracellular concentration of Rho-tagged SNAP-tag lacking an appended vehicle. ****$p \leq 0.0001$, ***$p \leq 0.001$, **$p \leq 0.01$, *$p \leq 0.05$; one-way ANOVA followed by post hoc Dunnett's test.

Imperfect Correlation between Overall Uptake and Cytosolic Localization of SNAP-tag Conjugates. When examined by FCS, the SNAP-tag conjugates studied fall into two categories with respect to whether they reach the cell cytosol after a 30 min incubation: those that accumulate to a detectable level compared to SNAP-Rho and those that do not (Figure 4B). SNAP-tag conjugates in the latter category include CPP9-SNAP-Rho, CPP12-SNAP-Rho, aPP5.3-SNAP-Rho, R8-SNAP-Rho, and ZiF-SNAP-Rho. Cells treated with 1 μM of these conjugates displayed a small (3−5-fold) but statistically insignificant increase in cytosolic localization relative to cells treated with SNAP-Rho, which accumulated in the cytosol to reach a concentration of 1.8 ± 0.20 nM. Cells treated with Pen-SNAP-Rho yielded a statistically significant increase in cytosolic fluorescence that correlated with intracellular concentrations between 5 and 65 nM, with an average of 23 ± 2.9 nM. FCS measurements revealed that the cytosolic concentration achieved by ZF5.3-SNAP-Rho was at least 2-fold higher than that measured for Pen-SNAP-Rho, and more than 6-fold higher than the concentration measured for any other SNAP-tag conjugate tested. For ZF5.3-SNAP-Rho, the calculated cytosolic concentration after a 30 min incubation ranged from 14 to 144 nM, with an average of 58 ± 6.1 nM. Overall, our results demonstrate that both ZF5.3 and Pen are effective vehicles for delivering SNAP-tag into the cytosol of Saos-2 cells.

Effects of Concentration and Time. Next, we made use of FCS to quantify the effects of concentration and incubation time on the cytosolic localization of two SNAP-tag conjugates: one that accesses the cytosol well (ZF5.3-SNAP-Rho) and one that does not (CPP12-SNAP-Rho) (Figure 5A). First, Saos-2 cells were treated with increasing concentrations of ZF5.3-SNAP-Rho or CPP12-SNAP-Rho (1−3 μM) for 30 min and analyzed by flow cytometry and FCS as previously described (Figure 5B). While we observed a dose-dependent increase in the total cellular uptake by flow cytometry when Saos-2 cells were treated with ZF5.3-SNAP-Rho (up to 4-fold), only a modest increase was observed when cells were treated with CPP12-SNAP-Rho (up to 2-fold). These trends are mirrored by the FCS data: cells treated with increasing concentrations of ZF5.3-SNAP-Rho showed a dose-dependent increase in cytosolic concentration as determined by FCS. Treatment concentrations of 1 and 2 μM ZF5.3-SNAP-Rho resulted in average cytosolic concentrations of 58 ± 6.1 nM and 110 ± 13 nM, respectively, corresponding to an average delivery efficiency of 6%. At the highest treatment concentration of 3 μM, we observed an average cytosolic concentration of 251 ± 34 nM, a delivery efficiency of 8%. In contrast, the cytosolic

DOI: 10.1021/acscentsci.8b00446
ACS Cent. Sci. 2018, 4, 1379−1393

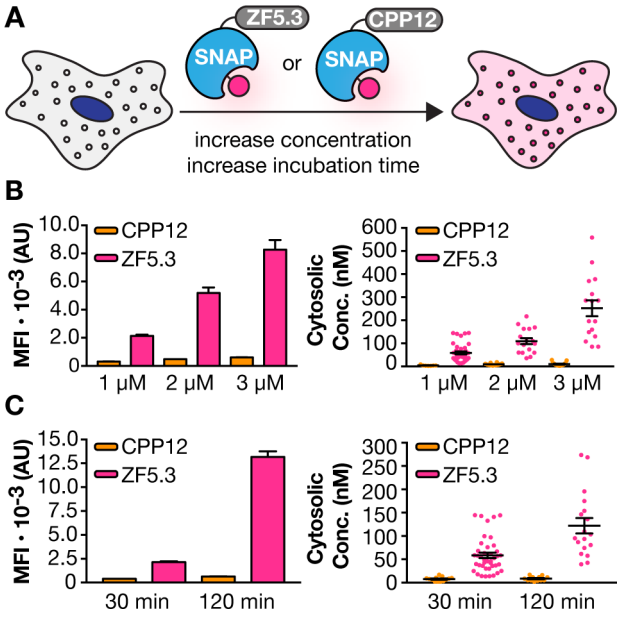

Figure 5. (A) Evaluation of the overall uptake and cytosolic delivery of ZF5.3-SNAP-Rho and CPP12-SNAP-Rho with increasing treatment concentration or time using flow cytometry and FCS. (B) Flow cytometry bar plots (left) indicating total levels of cellular uptake and scatter plot representation of cytosolic concentrations (right) determined by FCS for varying treatment concentrations (1, 2, or 3 μM) of either CPP12-SNAP-Rho or ZF5.3-SNAP-Rho. (C) Flow cytometry bar plots (left) indicating total levels of cellular uptake and scatter plot representation of cytosolic concentrations (right) determined by FCS with varying incubation times (30 or 120 min) of either CPP12-SNAP-Rho or ZF5.3-SNAP-Rho (treatment concentration 1 μM). MFI values represent the average median fluorescence intensity of cells determined from 3−12 individual replicates (10 000 cells each).

concentration of CPP12-SNAP-Rho did not significantly increase as a function of treatment concentration. At the highest concentration tested, the delivery efficiency of CPP12-SNAP-Rho was less than 1%.

In order to evaluate the effect of incubation time on cytosolic delivery, we treated Saos-2 cells with 1 μM solutions of ZF5.3-SNAP-Rho and CPP12-SNAP-Rho for 2 h (as opposed to 30 min) prior to analysis by flow cytometry and FCS (Figure 5C). Cells treated with ZF5.3-SNAP-Rho for 2 h and evaluated using flow cytometry exhibited a 6.5-fold increase in total intracellular fluorescence relative to cells treated with the same concentration for 30 min; under these conditions the cytosolic levels of ZF5.3-SNAP-Rho determined using FCS increased by a factor of 2 (117 ± 19 nM). Cells treated with CPP12-SNAP-Rho for 2 h and evaluated using flow cytometry exhibited a 2-fold increase relative to cells treated with CPP12-SNAP-Rho for 30 min. However, in contrast to results obtained using ZF5.3-SNAP-Rho, we were unable to detect a significant increase in the cytosolic concentration of CPP12-SNAP-Rho after prolonged incubation times. Taken as a whole, these studies demonstrate that FCS can be used to precisely examine the effects of treatment concentration and incubation time on the delivery of protein cargo into the cytosol, and that the extent of cytosolic localization cannot be predicted by flow cytometry alone.

Ensuring Delivery of Active Enzymes. Next, we devised an *in cellulo* assay to evaluate whether an unlabeled SNAP-tag conjugate would retain self-labeling activity following intracellular delivery (Figure 6A). We treated cells with 3 μM of each unlabeled uCPP, CPMP, or cCPP SNAP-tag conjugate

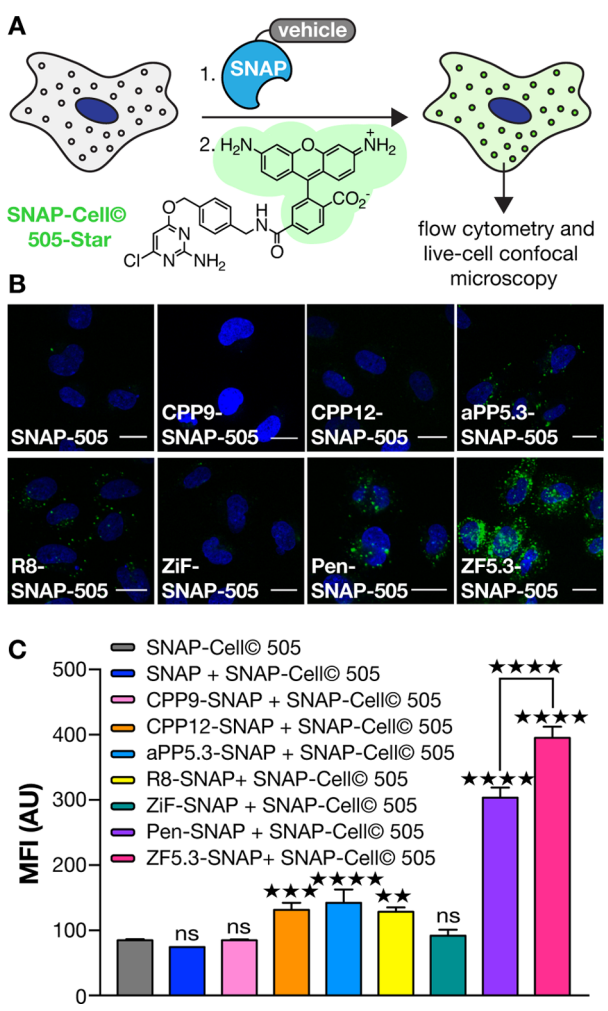

Figure 6. Evaluation of SNAP-tag activity *in cellulo*. (A) Scheme depicting *in cellulo* labeling of SNAP-tag conjugate proteins with SNAP-Cell© 505-Star. Saos-2 cells were incubated with 3 μM of each unlabeled SNAP-tag conjugate for 30 min followed by treatment with 1 μM SNAP-Cell© 505-Star for 45 min. Intracellular fluorescence was assessed using confocal microscopy and flow cytometry. (B) Confocal microscopy images of live cells treated with each indicated SNAP-tag conjugate and SNAP-Cell© 505-Star as described above. Scale bar = 20 μm. (C) Flow cytometry bar plots illustrating relative levels of total intracellular fluorescence resulting from treatment with each SNAP-tag conjugate followed by SNAP-Cell© 505-Star. MFI values represent the average median fluorescence intensity of cells determined from three individual replicates (10 000 cells each). MFI values corresponding to each SNAP-tag conjugate were compared to cells incubated with blank media (no added conjugate) followed by SNAP-Cell© 505-Star. ****$p \leq 0.0001$, ***$p \leq 0.001$, **$p \leq 0.01$, *$p \leq 0.05$; one-way ANOVA followed by post hoc Dunnett's test.

for 30 min, washed the cells with DPBS (Dulbecco's phosphate buffered saline), and performed the labeling reaction *in cellulo* by incubating the cells in media containing 1 μM SNAP-Cell© 505-Star for an additional 45 min. After the labeling period, the cells were incubated with fresh media for 30 min to remove unreacted SNAP-Cell© 505-Star, washed with DPBS, lifted with trypsin, and imaged using confocal microscopy (Figure 6B). Cells treated with SNAP, CPP9-SNAP, and ZiF-SNAP

DOI: 10.1021/acscentsci.8b00446
ACS Cent. Sci. 2018, 4, 1379−1393

displayed no significant intracellular fluorescence after treatment with SNAP-Cell© 505-Star. Cells treated with CPP12-SNAP displayed low levels of punctate fluorescence, whereas cells treated with aPP5.3-SNAP and R8-SNAP displayed bright punctate fluorescence. Cells treated with Pen-SNAP and ZF5.3-SNAP exhibited exceptionally bright punctate fluorescence and low levels of diffuse cytosolic staining. We then quantitatively compared the levels of intracellular fluorescence (endosomes plus cytosol) after treatment with SNAP-Cell© 505-Star using flow cytometry (Figure 6C). Overall, there is good agreement between the results of flow cytometry and confocal microscopy. Cells treated with Pen-SNAP and ZF5.3-SNAP and subsequently incubated with SNAP-Cell© 505-Star were approximately 3.6- and 4.7-fold brighter, respectively, than cells treated with SNAP-Cell© 505-Star alone. While we intended to measure the precise concentration of each SNAP-tag conjugate after labeling *in cellulo* using FCS, we were unable to completely remove unreacted SNAP-Cell© 505-Star (or three other fluorescent SNAP-tag substrates) from the cytosol in untreated control samples and were concerned by the heterogeneous nature of the acquired traces. Notwithstanding this limitation, the confocal microscopy and flow cytometry measurements confirm that delivered SNAP-tag retains its activity in cells, despite its travels through the endosomal pathway.[82] Overall, the level of *in cellulo* SNAP-tag activity exhibited by a given SNAP-conjugate correlates well with cytosolic delivery (determined by FCS). The minor discrepancies between these experiments could result, for example, from subtle differences in SNAP-tag activity that depend on CPP identity, or from a dye-dependent conformational change that alters CPP efficacy, or a combination of these (or other) effects.

Delivery of Diverse Cargo. To demonstrate that FCS can be used to monitor the cytosolic trafficking of an enzyme other than SNAP-tag, we turned to the enzyme APEX2. APEX2 (28 kDa) is a monomeric, heme-binding, H_2O_2-dependent peroxidase that is highly active in the mammalian cell cytosol.[68,83] We began by expressing variants of APEX2 and a ZF5.3-APEX2 fusion protein that each carried a C-terminal His tag and a sortase recognition motif to enable site-specific tagging with a Rho-containing peptide (NH_2-G_3K-Rho, Figure S6).[84] While we attempted to express APEX2 variants containing two of the more inefficient uCPPs—R8 and Tat—both could be expressed in only very low yield and precipitated during dialysis; further optimization was not pursued. APEX2, ZF5.3-APEX2, APEX2-LPETGG, and ZF5.3-APEX2-LPETGG were overexpressed in *E. coli* and purified by IMAC. After being labeled with sortase, APEX2-Rho and ZF5.3-APEX2-Rho were purified to homogeneity (see Methods for details). The identity and purity of APEX2, ZF5.3-APEX2, APEX2-Rho, and ZF5.3-APEX2-Rho were assessed by MS and SDS-PAGE, respectively (Figure S7). The levels of heme-bound enzyme were determined spectroscopically as described by Lam et al.[68] To ensure that the prepared enzymes were active, we compared the activity of APEX2 and ZF5.3-APEX2 to APEX2-Rho and ZF5.3-APEX2-Rho using a previously reported colorimetric guaiacol oxidation assay and found that all four enzymes exhibit robust peroxidase activity *in vitro* (Figure S8).[68]

Quantifying Total Cellular Uptake and Cytosolic Localization of APEX2. With a set of Rho-tagged APEX2 enzymes in hand, we first evaluated their total uptake into cells using confocal microscopy (Figure 7A) and flow cytometry

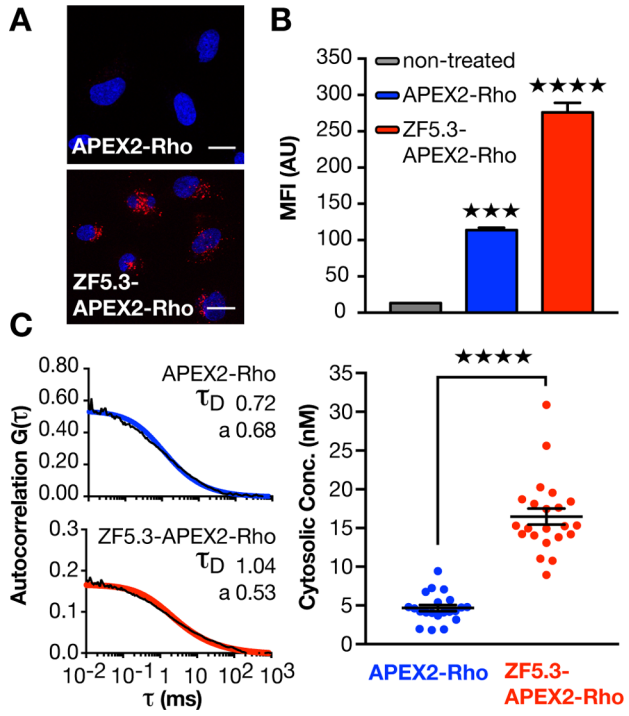

Figure 7. Assessment of ZF5.3-mediated delivery of APEX2-Rho. (A) Confocal microscopy images of live Saos-2 cells treated with 1 μM of each APEX2 conjugate for 30 min with the indicated Rho-tagged SNAP-tag conjugate. Scale bar = 20 μm. (B) Flow cytometry bar plots illustrating the relative uptake of each Rho-tagged APEX2 conjugate after 30 min incubation and treatment with trypsin. MFI values represent the average median fluorescence intensity of cells determined from three individual replicates (10 000 cells each). Error bars represent the standard error of the mean. MFI values corresponding to each SNAP-tag conjugate were statistically compared to nontreated cells. (C) Representative *in cellulo* FCS traces (left) corresponding to each indicated Rho-tagged APEX2 conjugate displaying the diffusion time (τ_D) as well as the anomalous coefficient (a) associated with each representative trace and scatter plot representation (right) of intracellular concentrations of Rho-tagged APEX2 conjugates determined from respective autocorrelation fits. ****$p \leq 0.0001$, ***$p \leq 0.001$, **$p \leq 0.01$, *$p \leq 0.05$; one-way ANOVA followed by post hoc Dunnett's test.

(Figure 7B). Saos-2 cells were treated with 1 μM of each labeled enzyme for 30 min and prepared for confocal microscopy and flow cytometry measurements in the same manner as described for SNAP-tag. Cells treated with 1 μM APEX2-Rho displayed minimal levels of punctate fluorescence, whereas cells treated with 1 μM ZF5.3-APEX2-Rho displayed much brighter, though predominantly punctate, intracellular fluorescence. Further analysis by flow cytometry revealed that cells treated with ZF5.3-APEX2-Rho were 2.4-fold brighter than cells treated with APEX2-Rho, confirming that the appended miniature protein enhances the total uptake of APEX2 into cells. We then quantified the amount of APEX2-Rho and ZF5.3-Rho that reaches the cytosol using FCS (Figure 7C). The average diffusion times (τ_D) of ZF5.3-APEX2-Rho and APEX2-Rho measured in the cytosol were 0.65 ± 0.057 and 0.95 ± 0.12 ms, respectively, approximately 4- and 6-fold longer than values acquired *in vitro* and at least 3-fold longer than the intracellular diffusion time measured for ZF5.3^R (Figure S9). FCS measurements revealed that the intracellular concentrations achieved by ZF5.3-APEX2-Rho

DOI: 10.1021/acscentsci.8b00446
ACS Cent. Sci. 2018, 4, 1379−1393

ranged from 9 to 30 nM, with an average intracellular concentration of 17 ± 1.0 nM, whereas the intracellular concentration of APEX2-Rho ranged from 2 to 9 nM, with an average of 4.7 ± 0.41 nM. The overall uptake and cytosolic concentration of ZF5.3-APEX2-Rho were lower compared to ZF5.3-SNAP-Rho, demonstrating the impact of cargo on the potency of the appended CPMP. Certainly, more work is needed to correlate cargo and CPP identity with the efficiency of cytosolic access and characterize in more detail the precise mechanism(s) by which endosomal escape occurs.

Evaluating the Activity of APEX2 Activity in Cells. To evaluate whether APEX2 retained activity upon delivery to the cytosol by ZF5.3, we made use of an assay developed by Ting et al.[68] that monitors the APEX2-dependent oxidation and fluorescence turn-on of the cell-permeant dye Amplex UltraRed (Figure 8A). Saos-2 cells were incubated with 500 nM of heme-bound APEX2 or ZF5.3-APEX2 for 30 min, treated with trypsin to remove surface-bound enzyme, transferred to microcentrifuge tubes, and resuspended in 100 μL of DPBS containing 10 μM of Amplex UltraRed and 1 mM H_2O_2. After 1 min, intracellular fluorescence was analyzed using flow cytometry (Figure 8B). Cells treated with ZF5.3-APEX2 exhibited a 13-fold turn-on of fluorescence relative to cells treated with Amplex UltraRed alone, whereas cells treated with APEX2 exhibited only a 1.2-fold increase in fluorescence. To visualize the APEX2-dependent turn-on of Amplex UltraRed fluorescence in live cells, we performed a similar experiment but visualized cells individually using confocal microscopy (Figure 8C). Cells treated with ZF5.3-APEX2 displayed exceptionally bright punctate and cytosolic fluorescence, whereas cells treated with APEX2 did not exhibit any significant turn-on of Amplex UltraRed within the same imaging time frame. Although these assays demonstrate that ZF5.3-APEX2-His_6 is active in cells, we acknowledge that the pattern of Amplex UltraRed fluorescence may not accurately depict the intracellular location of ZF5.3-APEX2-His_6; Amplex UltraRed that is oxidized in endosomal compartments by entrapped ZF5.3-APEX2-His_6 may also diffuse into the cytosol. Regardless, these results demonstrate that the CPMP ZF5.3 can deliver active APEX2 into cells. Moreover, these results emphasize the limited extent to which APEX2 activity—which, by nature, is amplified—correlates with the relative levels of APEX2 enzymes in the cell cytosol determined by FCS.

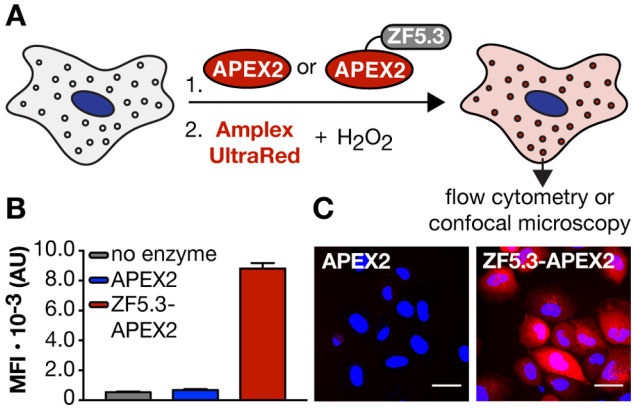

Figure 8. Evaluation of APEX2 activity *in cellulo* by flow cytometry and confocal microscopy using Amplex UltraRed. (A) Scheme depicting assay for assessing APEX2 activity *in cellulo* with Amplex UltraRed. Saos-2 cells were incubated with 500 nM of each APEX2 conjugate for 30 min followed by treatment with 10 μM Amplex UltraRed and 1 mM H_2O_2 for 1 min. Intracellular fluorescence was assessed using confocal microscopy and flow cytometry. (B) Flow cytometry bar plots representing the levels of intracellular Amplex UltraRed fluorescence. MFI values represent the average median fluorescence intensity of cells determined from three individual replicates (10,000 cells each). Error bars represent the standard error of the mean. (C) Confocal microscopy images of live cells treated with 500 nM of each indicated APEX2 conjugate followed by 10 μM Amplex UltraRed, and 1 mM H_2O_2 for 1 min. Scale bar = 20 μm.

CONCLUSIONS

Cell-penetrating peptides,[13] supercharged proteins,[85−87] synthetically surface-modified proteins,[29,88,89] bacterial toxins,[90] cationic lipids,[49] induced transduction systems,[39] and nanoparticles[44,45] have all been evaluated as strategies for delivering functional protein cargo into cells. Despite the increasing number of reported methods for protein delivery, most assays used to assess trafficking into the cytosol are qualitative and indirect and can therefore be misleading. These limitations make evaluating progress in the field of protein delivery extremely challenging. In this work, we applied our previously described FCS method[47] to directly quantify the relative efficiencies with which uCPPs, CPMPs, and synthetic cCPPs transport a model self-labeled enzyme into cell cytosol. Unlike any other reported strategy for assessing protein delivery, FCS yields direct and precise measurements of cytosolic concentrations in living cells in real-time. Importantly, we found that the extent of cytosolic trafficking of protein cargo cannot be ascertained accurately using confocal microscopy, flow cytometry, or enzymatic activity assays—the compartmental resolution and precision afforded by FCS were required to distinguish conjugates that accumulate in the cytosol in appreciable levels from those that do not.

Many of the differences between FCS and other, perhaps less technical, assays stem from the fact that CPP-mediated protein delivery into cell cytosol, in most cases, requires at least two distinct steps: uptake by endocytosis and then endosomal release. While many CPP−protein conjugates are readily endocytosed, most fail to reach the cytosol due to endosomal entrapment. In our study, we found that the cytosolic concentrations measured by FCS correlated poorly with overall uptake, suggesting that there are fundamental differences in the ability of each SNAP-tag conjugate to escape the endocytic pathway. To more carefully assess endosomal escape efficiency, we calculated an "endosomal escape ratio" (EER) for each conjugate, which corresponds to the concentration of a CPP−Snap-tag conjugate that reaches the cytosol divided by the overall uptake as determined by flow cytometry, and compared these values to SNAP-tag lacking an appended vehicle (Figure S10). This analysis revealed that only two molecules, the miniature protein ZF5.3 and the cyclic peptide CPP9 promoted the endosomal release of SNAP-tag conjugate significantly over background. Although the EER value calculated for CPP9-SNAP-Rho is 1.3-fold higher than that of ZF5.3-SNAP-Rho, the cytosolic concentration it achieves is 9.6-fold lower (Figure 4B). While we appreciate that this finding is likely cargo-dependent, it does emphasize that the combination of flow cytometry and FCS can be used to evaluate the endosomal escape efficiency of any conjugate of interest, provided that the molecule under study can be site-specifically labeled with an appropriate fluorophore. We anticipate that FCS techniques will dramatically accelerate

DOI: 10.1021/acscentsci.8b00446
ACS Cent. Sci. 2018, 4, 1379−1393

our ability to identify, evaluate, and optimize current strategies for delivering large, intact proteins to intracellular locales.

METHODS

Safety Statement. No unexpected or unusually high safety hazards were encountered.

Plasmid Cloning. Genes encoding ZF5.3-SNAP-His_6, aPP5.3-SNAP-His_6, TAT-SNAP-His_6, R8-SNAP-His_6, ZiF-SNAP-His_6, G_3-SNAP-His_6, SrtA7M-StrepTagII, APEX2-His_6, and ZF5.3-APEX2-LPETGG-His_6 were codon-optimized for expression in *E. coli* and purchased as synthetic double-stranded gBlocks (IDT) for plasmid construction using Gibson assembly.[91] Each synthetic gBlock was incorporated into a linearized pET vector (originally pET32A) containing complementary overhangs using commercial Gibson assembly reagents and protocols. The sequences of the synthetic gBlocks and primers used for generating additional expression plasmids (SNAP-His_6, MIEGR-G_3-SNAP-His_6, APEX2-His_6, ZF5.3-APEX2-His_6, and APEX2-His_6-LPETGG) are listed in the Supporting Information.

Expression and Purification of SNAP-His_6 Constructs. Plasmids encoding each His-tagged SNAP-tag conjugate were individually used to transform *E. coli* BL21(DE3) cells. Individual colonies were selected on the basis of Ampicillin (Amp) resistance and used to inoculate 5 mL of lysogeny broth (LB) media supplemented with Amp (100 mg/L). The primary cultures were used to inoculate 1 L of LB medium supplemented with Amp, which was then allowed to grow at 37 °C with shaking at 200 rpm. When the OD_{600} reached 0.6–0.8, the culture was cooled to 18 °C. Protein expression was induced by the addition of IPTG to a final concentration of 1 mM. After 16 h, the cells were harvested by centrifugation and lysed by sonication in 20 mM Tris pH 8.0, 150 mM NaCl, and 10% glycerol, supplemented with one cOmplete, Mini EDTA-free protease inhibitor cocktail tablet. The cleared lysate was obtained by centrifugation at 15000*g* for 30 min. Next, the cleared lysate was incubated with 2 mL of Ni-NTA resin for 1 h at 4 °C. After the resin/lysate mixture was transferred to a column, the resin was washed with high-salt wash buffer (20 mM Tris pH 8.0, 1 M NaCl, 30 mM imidazole, and 10% glycerol, 2 × 20 mL) followed by a low-salt wash (20 mM Tris pH 8.0, 150 mM NaCl, and 10% glycerol, 2 × 20 mL). The proteins were eluted in eight 1 mL portions of 20 mM Tris pH 8.0, 150 mM NaCl, 250 mM imidazole, and 10% glycerol. Elution fractions were analyzed by SDS-PAGE, combined, and dialyzed into 20 mM Tris pH 8.0, 150 mM NaCl, 1 mM DTT, and 10% glycerol overnight at 4 °C. ZiF-SNAP-His_6 and ZF5.3-SNAP-His_6 were dialyzed into the same buffer supplemented with 100 μM of $ZnCl_2$. Following dialysis, each protein was analyzed by mass spectrometry. We observed that a portion of the expressed ZF5.3-SNAP-His_6 contained an oxidative modification corresponding a mass increase of 80 Da. Purified ZF5.3-SNAP-His_6 was buffer exchanged into Zn-free SNAP-tag buffer (20 mM Tris pH 8.0, 150 mM NaCl, containing 10% glycerol). Bond-breaker tris(2-carboxyethyl) (TCEP) solution was added to 3 mL of 50 μM ZF5.3-SNAP-His_6 to a final concentration of 50 mM. The protein solution containing the added reducing agent was incubated overnight at 37 °C. Removal of the 80 Da adduct was confirmed by mass spectrometry. After removal of the 80 Da adduct, TCEP was removed from the reaction mixture using a PD-10 column. The protein was then redialyzed into SNAP-tag buffer supplemented with 100 μM $ZnCl_2$ overnight at 4 °C. Protein concentrations were assessed using the Pierce 660 nm protein assay and stored at −80 °C until further use.

Expression and Purification of SrtA7M-StrepTagII. The plasmid encoding SrtA7M-StrepTagII was used to transform *E. coli* BL21(DE3) cells. Individual colonies were selected on the basis of Amp resistance and used to inoculate 50 mL of LB media supplemented with Amp (100 mg/L). The primary culture was grown overnight and then used to inoculate 2 L of LB medium supplemented with Amp, which was then allowed to grow at 37 °C with shaking at 200 rpm. When the OD_{600} reached 0.5, the protein expression was induced by the addition of IPTG to a final concentration of 1 mM. After 4 h, the cells were harvested by centrifugation and lysed by sonication in 20 mM Tris pH 8.0, 150 mM NaCl, and 10% glycerol, supplemented with one cOmplete, Mini EDTA-free protease inhibitor cocktail tablet. The cleared lysate was obtained by centrifugation at 15000*g* for 30 min. Next, the cleared lysate was manually added to a 5 mL StrepTrap HP column. After the lysate was transferred to a column, the column was washed with 30 mL of 20 mM Tris pH 8.0, 150 mM NaCl, and 10% glycerol. After the column was washed, SrtA7M-StrepTagII was eluted from the resin using 20 mM Tris pH 8.0, 150 mM NaCl, and 10% glycerol supplemented with 2 mM of desthiobiotin in eight 2 mL portions. Elution fractions were analyzed by SDS-PAGE, combined, and dialyzed into 20 mM Tris pH 8.0, 150 mM NaCl, 1 mM DTT, and 10% glycerol. Protein concentrations were assessed using the Pierce 660 nm protein assay and stored at −80 °C until further use.

Expression and Purification of APEX2-His_6 Constructs. Plasmids encoding each His-tagged APEX2 conjugate were used to transform *E. coli* BL21(DE3) cells. Individual colonies were selected on the basis of Amp resistance and used to inoculate 5 mL of LB media supplemented with Amp (100 mg/L). The primary cultures were used to inoculate 1 L of LB medium supplemented with Amp, which was then allowed to grow at 37 °C with shaking at 200 rpm. When the OD_{600} reached 0.4, the culture was cooled to 25 °C. Protein expression was induced by the addition of IPTG to a final concentration of 0.4 mM. At this time, the media were also supplemented with 1 mM 5-aminolevulinic acid to promote heme biosynthesis. After 16 h, the cells were harvested by centrifugation and lysed by sonication in 20 mM Tris pH 8.0, 150 mM NaCl, and 10% glycerol, supplemented with one cOmplete, mini EDTA-free protease inhibitor cocktail tablet. The cleared lysate was obtained by centrifugation at 15000*g* for 30 min. Next, the cleared lysate was incubated with 2 mL of Ni-NTA resin for 1 h at 4 °C. After the resin/lysate mixture was transferred to a column, the resin was washed with high-salt wash buffer (20 mM Tris pH 8.0, 1 M NaCl, 30 mM imidazole, and 10% glycerol, 2 × 20 mL) followed by a low-salt wash (20 mM Tris pH 8.0, 150 mM NaCl, and 10% glycerol, 2 × 20 mL). The proteins were eluted in eight 1 mL portions of 20 mM Tris pH 8.0, 150 mM NaCl, 250 mM imidazole, and 10% glycerol. Elution fractions were analyzed by SDS-PAGE, combined, and dialyzed into 20 mM Tris pH 8.0, 150 mM NaCl, 1 mM DTT, 10% glycerol, and 100 μM $ZnCl_2$ overnight at 4 °C. Total protein concentrations were assessed using the Pierce 660 nm protein assay and stored at −80 °C until further use.

Synthesis of CPP9/12-PEG_2-$LPETG_3$ Peptides. The synthesis of CPP9-PEG_2-$LPETG_3$ and CPP12-PEG_2-$LPETG_3$ was based on the method previously reported by Qian et al.[76] CPP9-PEG_2-$LPETG_3$ and CPP12-PEG_2-$LPETG_3$ precursor

DOI: 10.1021/acscentsci.8b00446
ACS Cent. Sci. 2018, 4, 1379−1393

peptides were synthesized on H-Rink Amide-ChemMatrix resin using a Biotage Alstra automated microwave peptide synthesizer. Each coupling reaction was performed using 5 equiv of Fmoc-protected amino acid, 5 equiv of 2-(1*H*-benzotriazol-1-yl)-1,1,3,3-tetramethyluronium hexauorophosphate (HBTU), 5 equiv of 1-hydroxybenzotriazole (HOBt), and 10 equiv of *N*,*N*-diisopropylethylamine (DIPEA) in dimethylformamide (DMF). Fmoc deprotections were performed using 20% piperidine in DMF. Following microwave synthesis, the resin was transferred to a glass peptide synthesis vessel, purged with nitrogen, and washed with anhydrous dichloromethane (DCM). The Glu(OAll) side chain was deprotected (3 × 20 min) using 0.1 equiv of $Pd(PPh_3)_4$ and 10 equiv of phenylsilane in anhydrous DCM. Next, the *N*-terminal Fmoc residue was deprotected using 20% piperidine in DMF (2 × 10 min). Following the deprotection steps, the peptide was cyclized by stirring the resin with 10 equiv of benzotriazol-1-yl oxytripyrrolidinophosphonium hexafluorophosphate (PyBOP) and 20 equiv of DIPEA overnight. The peptides were deprotected and cleaved from the resin by stirring the resin in 88% trifluoroacetic acid, 5% triisopropyl silane, 5% phenol, and 2% water for 2 h at room temperature. Finally, the peptides were precipitated in cold diethyl ether, isolated by centrifugation, and purified by reversed-phase HPLC over a semiprep Grace Vydac C18 (218TP) column. The identity of each peptide was confirmed by mass spectrometry.

Sortase-Mediated Synthesis of CPP9/CPP12-SNAP-Tag-His_6. MIEGR-G_3-SNAP-His_6 was overexpressed, purified by immobilized metal ion chromatography as described above, and dialyzed into Factor Xa cleavage buffer (20 mM Tris pH 7.0, 150 mM NaCl, 2 mM $CaCl_2$, 10% glycerol) overnight at 4 °C. Quantitative cleavage of the *N*-terminal MIEGR sequence was achieved by incubating 10 mg of the purified protein with 50 μg of commercial Factor Xa (NEB) overnight at 30 °C. Following removal of the *N*-terminal MIEGR fragment, Factor Xa was inactivated by the addition of 1 mM TCEP. The cleaved protein was then dialyzed into 20 mM Tris pH 8.0, 150 mM NaCl, 1 mM DTT, and 10% glycerol for 4 h at 4 °C. To generate CPP9-SNAP-His_6 and CPP12-SNAP-His_6, G_3-SNAP-His_6 (100 μM) was incubated with SrtA7M-StrepTagII (75 μM) and HPLC purified CPP9-$LPETG_3$ or CPP12-$LPETG_3$ (200 μM) in 2 mL of 20 mM Tris pH 8.0, 150 mM NaCl, 1 mM DTT, and 10% glycerol. Reaction progress was monitored by LC-MS. After 1 h, good conversion (∼50%) to CPP9-SNAP-His_6 and CPP12-SNAP-His_6 was observed. However, further optimization of the reaction conditions proved difficult. Increasing the concentration of CPP9-$LPETG_3$ (up to 500 μM) resulted in significant precipitation of the reaction. Increasing the concentration of SrtA7M-StrepTagII (up to 150 μM) or allowing the reaction to proceed for longer periods of time (up to 4 h) resulted in reduced formation of the desired conjugate. We therefore employed a two-step purification strategy to obtain CPP9-SNAP-His_6 and CPP12-SNAP-His_6 from a partially labeled mixture with exceptional purity. First, the reaction mixture was incubated with 500 μL of Ni-NTA resin for 30 min at 4 °C. The resin was then washed (2 × 10 mL) with high salt buffer (20 mM Tris pH 8.0, 1 M NaCl, 1 mM DTT, and 10% glycerol) to remove CPP9-$LPETG_3$ or CPP12-$LPETG_3$ and SrtA7M-StrepTagII. An additional wash was performed with SNAP-tag buffer (20 mM Tris pH 8.0, 150 mM NaCl, 1 mM DTT, and 10% glycerol). The His_6 tagged proteins (G_3-SNAP-His_6 and CPP9-SNAP-His_6 or CPP12-SNAP-His_6) were then eluted from the resin using SNAP-tag buffer supplemented with 250 mM imidazole. Next, G_3-SNAP-His_6 and CPP9-SNAP-His_6 or CPP12-SNAP-His_6 were purified over a HiTrapSP HP column using a 60 min NaCl gradient (0−1.0 M NaCl in 20 mM HEPES, pH 7.0). The product fractions were pooled, concentrated, and dialyzed into 20 mM Tris pH 8.0, 150 mM NaCl, 1 mM DTT, and 10% glycerol overnight at 4 °C. The identity and purity of isolated CPP9-SNAP-His_6 and CPP12-SNAP-His_6 were assessed by mass spectrometry and SDS-PAGE, respectively.

Synthesis of BG-Rho for SNAP-Tag Labeling. BG-amine was synthesized in accordance with Keppler et al.[67] To generate BG-Rho, BG-amine (3 mg, 9.8 μmol) was dissolved in 500 μL of anhydrous dimethyl sulfoxide (DMSO) and stirred with 3 equiv of lissamine rhodamine B sulfonyl chloride (11 mg, 29.4) in the presence of excess diisopropylamine (10.2 μL, 58.8 μmol) at room temperature overnight. BG-Rho was purified from the reaction mixture by reversed-phase HPLC over a semiprep Grace Vydac C18 (218TP) column and analyzed by mass spectrometry. HPLC fractions containing BG-Rho were combined, dried under reduced pressure, and resuspended in DMSO to yield 2 mM stock solutions for SNAP-tag labeling experiments.

Preparation of Rho-Tagged SNAP-Tag Proteins. One milliliter of a 20−40 μM solution of each purified SNAP-tag conjugate was incubated with 1.5 molar equiv of BG-Rho for 2 h at 37 °C. The labeling reaction was monitored using mass spectrometry. After the labeling reaction had gone to completion, excess dye was removed from the protein sample by exchanging the reaction buffer over a standard PD-10 desalting column. To ensure complete removal of undetectable remaining BG-Rho, the proteins were dialyzed overnight at 4 °C into 20 mM Tris, 150 mM NaCl, containing 10% glycerol and 1 mM DTT. Following dialysis, SNAP-Rho proteins were quantified using an extinction coefficient of lissamine rhodamine B (Rho) measured in water (112 000 M^{-1} cm^{-1}).

Synthesis of NH_2-G_3K-Rho. The Fmoc-Gly-Gly-Gly-Lys(Mtt) precursor peptide was synthesized on H-Rink Amide-ChemMatrix resin using a Biotage Alstra automated microwave peptide synthesizer as described above. Following synthesis, the resin was transferred to a glass peptide synthesis vessel and washed extensively with DCM. Deprotection of Mtt was achieved by stirring the resin in 2% TFA in DCM (3 × 15 min). Next, the peptide reaction vessel was purged with nitrogen and the resin was washed with anhydrous DMF and labeled with lissamine rhodamine B sulfonyl chloride as described above. After the labeling reaction, the *N*-terminal Gly residue was deprotected using 20% piperidine in DMF (2 × 15 min). The resin was then washed, dried, and cleaved in 95% TFA containing 2.5% TIPS and 2.5% H_2O for 1 h. The peptide was then purified by reversed-phase HPLC over a semiprep Grace Vydac C18 (218TP) column. HPLC fractions containing the purified peptide were identified by mass spectrometry, frozen, and dried by lyophilization. The identity of the purified peptide was confirmed by mass spectrometry.

Sortase-Mediated Synthesis of APEX2-Rho and ZF5.3-APEX2-Rho. To generate APEX2-Rho and ZF5.3-APEX2-Rho, APEX2-LPETGG-His_6 and ZF5.3-LPETGG-His_6 (50 μM) were incubated with SrtA7M-StrepTagII (75 μM) and HPLC purified NH_2-G_3K-Rho (300 μM) in 2 mL of 20 mM Tris pH 8.0, 150 mM NaCl, 1 mM DTT, and 10% glycerol until quantitative labeling was observed by mass spectrometry. To isolate APEX2-Rho, the sortase labeling reaction mixture was exchange into low-salt buffer (20 mM

DOI: 10.1021/acscentsci.8b00446
ACS Cent. Sci. 2018, 4, 1379−1393

Tris, pH 8.0), loaded onto a HiTrapQ column, and purified over a 60 min NaCl gradient (0 to 1.0 M NaCl in 20 mM Tris, pH 8.0). The fractions containing APEX2-Rho were analyzed by SDS-PAGE, pooled, and exchanged into 20 mM Tris pH 8.0, 150 mM NaCl, 10% glycerol, 1 mM DTT, and 100 μM $ZnCl_2$ using a PD-10 desalting column. While we attempted the same approach to purify ZF5.3-APEX2-Rho, we found that the labeled protein did not bind to the HiTrapQ column. Alternatively, we found that ZF5.3-APEX2-Rho (lacking the His_6 tag) retained affinity for TALON resin. We therefore isolated ZF5.3-APEX2-Rho from the sortase labeling reaction by directly loading the mixture onto a HiTrap TALON column. The HiTrap TALON column was washed extensively (3 × 20 mL) with 20 mM Tris pH 8.0, 150 mM NaCl, and 10% glycerol. ZF5.3-APEX2-Rho was eluted from the resin over a 60 min imidazole gradient (0−250 mM imidazole in 20 mM Tris, pH 8.0). The fractions containing ZF5.3-APEX2-Rho were analyzed by SDS-PAGE, pooled, and exchanged into 20 mM Tris pH 8.0, 150 mM NaCl, 10% glycerol, 1 mM DTT, and 100 μM $ZnCl_2$ using a PD-10 desalting column. The identity and purity of isolated APEX2-Rho and ZF5.3-APEX2-Rho were assessed by mass spectrometry and SDS-PAGE, respectively.

Cell Culture. Saos-2, HeLa, and SK-HEP-1 cell stocks were purchased from the American Type Culture Collection (ATCC). Saos-2 cells were cultured in McCoy's 5A medium supplemented with 15% fetal bovine serum (FBS), sodium pyruvate (1 mM), penicillin (100 units/mL), and streptomycin (100 μg/mL). HeLa cells were cultured in DMEM supplemented with 10% FBS, penicillin (100 units/mL), and streptomycin (100 μg/mL). SK-HEP-1 cells were cultured in EMEM supplemented with 10% FBS, penicillin (100 units/mL), and streptomycin (100 μg/mL). All cell cultures were maintained at 37 °C in a humidified atmosphere at 5% CO_2.

Confocal Microscopy. Confocal microscopy experiments were performed on an inverted Zeiss LSM 880 laser scanning confocal microscope equipped with a Plan-Apochromat 40*x*/1.2 NA water immersion lens and a diode pumped solid-state 561 nm laser suitable for excitation of Rho. One day prior to performing uptake experiments, ∼40 000 Saos-2 cells in 1 mL of clear McCoy's 5A medium (no phenol red) containing 15% FBS were plated in 12-well tissue culture treated plates and allowed to adhere overnight. The following morning, the cells were washed three times with DPBS, and the media was replaced with 500 μL of clear McCoy's 5A medium containing 1 μM solutions (or 2 μM and 3 μM solutions of ZF5.3-SNAP-Rho and CPP12-SNAP-Rho as indicated in the titration experiments) of each Rho-tagged SNAP-tag or APEX2 conjugate. The cells were incubated for 25 min at 37 °C, after which the cells were treated with 300 nM Hoechst 33342 nuclear stain for 5 additional min. The cells were washed three times with DPBS prior to lifting with 500 μL of trypsin (TrypLE Express) for 5 min at 37 °C. The cells were then transferred to a 15 mL Falcon tube containing 1 mL of clear McCoy's medium supplemented with 15% FBS and pelleted at 500*g* for 2 min. The cells were then washed with 1 mL of DPBS and pelleted again at 500*g* for 2 min. Finally, the cells were suspended in 250 μL of clear DMEM medium and replated onto fibronectin-coated (diluted 1:100 in DPSB) glass microscopy dishes. The cells were allowed to adhere to the microscopy dish for 15 min prior to imaging.

Flow Cytometry. Flow cytometry measurements were performed using an Attune NxT flow cytometer equipped with a 561 nm laser for excitation of Rho. One day prior to performing uptake experiments, ∼40 000 Saos-2 cells in 1 mL of McCoy's 5A medium containing 15% FBS were plated into 12-well tissue culture treated plates and allowed to adhere overnight. The following morning, the cells were washed three times with DPBS, and the media was replaced with 500 μL of McCoy's 5A medium containing 1 μM solutions (or 2 μM and 3 μM solutions of ZF5.3-SNAP-Rho and CPP12-SNAP-Rho as indicated in the titration experiments) of each Rho-labeled SNAP-tag or APEX2 conjugate. The cells were incubated for 30 min at 37 °C. The cells were washed three times with DPBS prior to lifting with 500 μL of trypsin for 5 min at 37 °C. The cells were then transferred to a 15 mL Falcon tube containing 1 mL of McCoy's Media supplemented with 15% FBS and pelleted at 500*g* for 2 min. The cells were then washed by resuspension in DPBS and again pelleted at 500 *g* for 2 min. The cells were finally suspended in 100 μL of DPBS and transferred to microcentrifuge tubes prior to obtaining flow cytometry measurements.

Fluorescence Correlation Spectroscopy. FCS measurements were obtained using an inverted Zeiss LSM 880 laser scanning confocal microscope equipped with a C-Apochromat 40*x*/1.2 NA water immersion objective as well as a photon counting GaAsP detector. One day prior to performing uptake experiments, ∼40 000 Saos-2 cells in 1 mL of McCoy's 5A medium containing 15% FBS were plated into 12-well tissue culture treated plates and allowed to adhere overnight. The cells were treated with each Rho-labeled SNAP-tag or APEX2 protein, stained with Hoechst 33342 nuclear stain, and prepared for FCS in the exact manner as described for the confocal microscopy measurements. All FCS measurements were performed at 37 °C in media containing 25 mM HEPES. Prior to FCS measurements in cells, the focal volume of the microscope was measured using an Alexa 594 dye standard solution. To do so, the correction collar of the C-apochromat 40x/N1.2 water immersion objective was adjusted to the correct cover glass thickness of each 8-well microscopy dish. The cover glass thickness was measured with a digital micrometer (Mitutoyo, Aurora, IL). Then, the pinhole of the 561 nm laser was aligned in both the x and the y direction. FCS traces for a standard solution of Alexa 594 dye (100 nM) in water were recorded at 37 °C in the same 8-well dish used for *in cellulo* FCS experiments (no fibronectin coating for the Alexa 594 standard). Autocorrelation data were collected over 5-s intervals with 10 repeats. During *in cellulo* FCS measurements, the cells were scanned visually to identify locations for cytosolic focal volume placement; nuclear regions, as well as regions with high punctate signal (endosomes), were avoided. The FCS traces were fit to a 3D diffusion equation using a custom MATLAB script as previously described. Briefly, autocorrelation curves from *in vitro* measurements were fit to a 3D diffusion eq (eq 1):

$$G(\tau) = \frac{1}{N}\frac{1}{\left(1+\frac{\tau}{\tau_{diff}}\right)\sqrt{\left(1+\frac{S^2\tau}{\tau_{diff}}\right)}} \quad (1)$$

N is the average number of diffusing molecules in the effective confocal volume (V_{eff}) and τ_{diff} is the diffusion time, the average time a molecule takes to transit the laser focus. The shape factor S of the effective focal volume V_{eff} was determined from the fit of the autocorrelation function of Alexa 594 (12.5 nM) in water at 25 °C ($S = 0.2 \pm 0.007$) and was fixed for all

DOI: 10.1021/acscentsci.8b00446
ACS Cent. Sci. 2018, 4, 1379−1393

subsequent analyses at $S = 0.2$. V_{eff} was determined to be 0.66 ± 0.090 fL and was calculated according to eqs 2 and 3:

$$\omega_1 = \sqrt{(4D\tau_{diff})} \tag{2}$$

$$V_{eff} = \pi^{3/2}\omega_1^3\frac{1}{S} \tag{3}$$

D is the diffusion coefficient of Alexa 594 at 37 °C (5.20×10^{-6} cm^2 s^{-1}), and τ_{diff} is the measured diffusion time (unit of time). The diffusion coefficient D of Alexa 594 at 37 °C was calculated using eq 4:

$$D\,(T) = D\,(25°C)\frac{t + 273.15}{\eta(t)}2.985 \times 10^{-6}\ \text{Pa·s·K}^{-1} \tag{4}$$

where $t = 37$ °C, D of Alexa 594 at is 25 °C (3.88×10^{-6} cm^2 s^{-1}),[92] and the viscosity η of water at 37 °C is 0.6913 m·Pa·s.

The final concentration C in the effective confocal volume V_{eff} was calculated as follows (eq 5):

$$C = \frac{N}{N_A V_{eff}} \tag{5}$$

where N_A is Avogardro's number (6.0221413×10^{23} mol^{-1}).

Autocorrelation curves from *in cellulo* measurements were fit to an anomalous diffusion model:

$$G(\tau) = \frac{1}{N}\frac{1}{\left(1 + \frac{\tau}{\tau_{diff}}\right)^{\alpha}\sqrt{\left(1 + S^2\frac{\tau}{\tau_{diff}}\right)^{\alpha}}} + G(\infty) \tag{6}$$

$G(\infty)$ represents the level of background autocorrelation at long time scales and α is the anomalous diffusion coefficient, which represents the degree to which diffusion is hindered over long distances.[93]

The fitted autocorrelation traces from live cell measurements were then evaluated and filtered as described before.[47] We discarded traces that displayed poor signal with counts per molecule (cpm) below 1 kHz and/or low anomalous diffusion coefficients ($\alpha < 0.3$).[94] With these parameters, we typically retained at least 75% of the collected data points.

Cytosolic Fractionation Assay. One day prior to performing uptake experiments, ∼5 million Saos-2 cells in 25 mL of McCoy's 5A medium containing 15% FBS were plated into T150 tissue culture flasks and allowed to adhere overnight. The following morning, the cells were washed three times with DPBS, and the media were replaced with 10 mL of clear McCoy's 5A medium containing a 1 μM solution of ZF5.3-SNAP-Rho or 10 mL of clear McCoy's 5A medium lacking added protein. The cells were incubated for 30 min at 37 °C, washed three times with DPBS, and lifted with 4 mL of trypsin. The cells were then transferred to 15 mL Falcon tubes containing 8 mL of clear McCoy's medium supplemented with 15% FBS and pelleted at 500*g* for 2 min. The cells were washed by resuspension with 3 mL of DPBS and pelleted at 500 g for 2 min. This step was repeated to perform a second wash. After the second DPBS wash, the cells were resuspended in 1 mL of precooled buffered isotonic sucrose buffer (290 mM sucrose, 10 mM imidazole pH 7.0, 1 mM DTT, and 1 cOmplete protease inhibitor cocktail per 10 mL buffer) and repelleted at 500*g* for 2 min. Next, the cells were suspended in 150 μL of isotonic sucrose, transferred to 0.5 mL microtubes containing 1.4 mm ceramic beads (Omni International) and homogenized using a Bead Ruptor 4 (Omni International) at speed 1 for 8 s. The homogenized cells were transferred to polycarbonate ultracentrifuge tubes and centrifuged at 350 kg for 30 min at 4 °C to isolate the cytosolic fraction. Next, the cytosolic fractions were boiled in gel loading buffer and separated by SDS-PAGE. The gel was analyzed by in-gel fluorescence scanning (Typhoon FLA 7000) prior to transfer onto PVDF membranes for Western blot analysis. SNAP-tag was detected by incubating the membrane with an anti-SNAP-tag antibody (New England Biolabs, Ipswich, MA) followed by incubation with an HRP-linked anti-Rabbit IgG antibody (Cell Signaling Technology, Danvers, MA). The HRP signal was developed using Clarity Western ECL Substrates (Bio-Rad, Hercules, CA).

Evaluating SNAP-Tag Activity *in cellulo*. One day prior to performing uptake experiments, ∼40 000 Saos-2 cells in 1 mL of McCoy's 5A medium containing 15% FBS were plated into 12-well tissue culture treated plates and allowed to adhere overnight. The following morning, the cells were washed three times with DPBS, and the media was replaced with 500 μL of clear McCoy's 5A medium containing 3 μM solutions of each unlabeled SNAP-tag protein. The cells were incubated for 30 min at 37 °C, washed three times with DPBS, and then treated with 500 nM SNAP-Cell© 505-Star in McCoy's 5A medium containing 15% FBS. After 40 min, the cells were treated with 300 nM Hoechst 33342 nuclear stain for 5 additional min. Next, the cells were washed three times with McCoy's 5A medium; to washout unreacted dye, the cells were incubated in fresh medium for an additional 30 min. Finally, the cells were lifted with trypsin, replated onto fibronectin-coated glass slides, and evaluated by confocal microscopy and flow cytometry as described above.

Guaiacol Oxidation Assay. First, the concentration of the heme-bound form of each enzyme (APEX2, ZF5.3-APEX2, APEX2-Rho, and ZF5.3-APEX2-Rho) was determined by absorption at 405 nm using a reported extinction coefficient corresponding to holo-APEX2.[68] APEX2, ZF5.3-APEX2, APEX2-Rho, and ZF5.3-APEX2-Rho enzymes were added to buffer (20 mM Tris pH 8.0, 150 mM NaCl, containing 10% glycerol) containing 1 mM guaiacol and 1 mM hydrogen peroxide (H_2O_2) to a final concentration of 500 nM. A sample lacking added APEX2 enzyme (buffer supplemented with 1 mM guaiacol and 1 mM H_2O_2) was prepared as a negative control. All samples were prepared in triplicate. After 5 min, the absorbance at 470 nm (corresponding to the oxidized tetraguaiacol product) was recorded using a Tecan Infinite M1000 plate reader.

Evaluating APEX2 Activity *in Cellulo*. One day prior to performing experiments, ∼40 000 Saos-2 cells in 1 mL of McCoy's 5A medium containing 15% FBS were plated into 12-well tissue culture treated plates and allowed to adhere overnight. The following morning, the cells were washed three times with DPBS, and the media was replaced with 500 μL of clear McCoy's 5A medium containing 500 nM solutions of heme-bound APEX2 and ZF5.3-APEX2 (1.8 μM and 1.1 μM total protein, respectively). Next, the cells were washed three times with DPBS, prior to lifting with 500 μL of trypsin (TrypLE Express) for 5 min at 37 °C. The cells were then transferred to a 15 mL Falcon tube containing 1 mL of clear McCoy's medium supplemented with 15% FBS and pelleted at 500*g* for 2 min. The cells were washed again with 1 mL of DPBS and pelleted at 500*g* for 2 min. The cells were then suspended in 100 μL of DPBS containing 10 μM of Amplex UltraRed and 1 mM H_2O_2. After 1 min, total intracellular

DOI: 10.1021/acscentsci.8b00446
ACS Cent. Sci. 2018, 4, 1379−1393

fluorescence was analyzed using flow cytometry. For confocal microscopy experiments, the cells were treated with each APEX2 enzyme as described above for 25 min followed by a 5 min incubation period with Hoechst 33342 nuclear stain. The cells were then washed and treated with trypsin as described above and transferred onto fibronectin-coated microscopy slides. After 20 min, 10 μM of Amplex UltraRed and 1 mM H_2O_2 were added directly to the wells and the cells were imaged immediately by confocal microscopy.

■ ASSOCIATED CONTENT

Supporting Information

The Supporting Information is available free of charge on the ACS Publications website at DOI: 10.1021/acscentsci.8b00446.

General information, plasmid cloning details, and figures describing protein purity analysis by SDS-PAGE and MS, flow cytometry experiments performed in HeLa and SK-HEP1 cells, *in vitro* FCS characterization of labeled proteins, APEX2 activity assays, and evaluation of the endosomal escape ratio corresponding to each SNAP-tag conjugate (PDF)

■ AUTHOR INFORMATION

Corresponding Author

*E-mail: alanna.schepartz@yale.edu.

ORCID

Alanna Schepartz: 0000-0003-2127-3932

Funding

This work was supported by a grant from Entrada Therapeutics. A.St. is grateful to the Howard Hughes Medical Institute for an International Student Research Fellowship. S.L.K. thanks the NIH for funding through the Chemistry-Biology Interface Training Program (T32GM06754).

Notes

The authors declare the following competing financial interest(s): The authors declare that A.S. and R.F.W. are named inventors of a pending patent application related to the work described.

■ ACKNOWLEDGMENTS

The authors thank Dr. Joe Wolenski for assistance with confocal microscopy, Dr. Garrett Cobb for development of the MATLAB script, and Dr. Chris Axline for further assistance with MATLAB. R.F.W. is grateful to Dr. Michael Witten for comments on the manuscript.

■ ABBREVIATIONS

aPP, avian pancreatic polypeptide; BG, benzyl guanine; cCPP, cyclic cell penetrating peptide; CP, chloropyrimidine; CPMP, cell-permeant miniature protein; CPP, cell-penetrating peptide; DPBS, Dulbecco's phosphate buffered saline; EER, endosomal escape ratio; FCS, fluorescence correlation spectroscopy; MFI, median fluorescence intensity; MS, mass spectrometry; Pen, penetratin; Rho, lissamine rhodamine B; uCPP, unstructured cell penetrating peptide; ZF, zinc finger

■ REFERENCES

(1) Usmani, S. S.; Bedi, G.; Samuel, J. S.; Singh, S.; Kalra, S.; Kumar, P.; Ahuja, A. A.; Sharma, M.; Gautam, A.; Raghava, G. P. S. Thpdb: Database of FDA-Approved Peptide and Protein Therapeutics. *PLoS One* **2017**, *12*, No. e0181748.

(2) Lagassé, H. A. D.; Alexaki, A.; Simhadri, V. L.; Katagiri, N. H.; Jankowski, W.; Sauna, Z. E.; Kimchi-Sarfaty, C. Recent Advances in (Therapeutic Protein) Drug Development. *F1000Research* **2017**, *6*, 113.

(3) Serna, N.; Sánchez-García, L.; Unzueta, U.; Díaz, R.; Vázquez, E.; Mangues, R.; Villaverde, A. Protein-Based Therapeutic Killing for Cancer Therapies. *Trends Biotechnol.* **2018**, *36*, 318−335.

(4) Marqus, S.; Pirogova, E.; Piva, T. J. Evaluation of the Use of Therapeutic Peptides for Cancer Treatment. *J. Biomed. Sci.* **2017**, *24*, 1−15.

(5) Gilroy, C. A.; Luginbuhl, K. M.; Chilkoti, A. Controlled Release of Biologics for the Treatment of Type 2 Diabetes. *J. Controlled Release* **2016**, *240*, 151−164.

(6) Li, P.; Zheng, Y.; Chen, X. Drugs for Autoimmune Inflammatory Diseases: From Small Molecule Compounds to Anti-Tnf Biologics. *Front. Pharmacol.* **2017**, *8*, 460.

(7) Ware, C. F. In *Adv. Pharmacol.*; Webb, D. R., Ed.; Academic Press: Cambridge, MA, 2013; Vol. *66*, pp 51−80.

(8) Ghosh, S. Biologic Therapies: Lessons from Multiple Sclerosis. *Dig. Dis.* **2012**, *30*, 383−386.

(9) Menge, T.; Weber, M. S.; Hemmer, B.; Kieseier, B. C.; von Budingen, H. C.; Warnke, C.; Zamvil, S. S.; Boster, A.; Khan, O.; Hartung, H. P.; Stuve, O. Disease-Modifying Agents for Multiple Sclerosis Recent Advances and Future Prospects. *Drugs* **2008**, *68*, 2445−2468.

(10) Bishop, P.; Lawson, J. Recombinant Biologics for Treatment of Bleeding Disorders. *Nat. Rev. Drug Discovery* **2004**, *3*, 684−694.

(11) Boustany, R.-M. N. Lysosomal Storage Diseases—the Horizon Expands. *Nat. Rev. Neurol.* **2013**, *9*, 583−598.

(12) Lachmann, R. H. Enzyme Replacement Therapy for Lysosomal Storage Diseases. *Curr. Opin. Pediatr.* **2011**, *23*, 588−593.

(13) Bolhassani, A.; Jafarzade, B. S.; Mardani, G. In Vitro and in Vivo Delivery of Therapeutic Proteins Using Cell Penetrating Peptides. *Peptides* **2017**, *87*, 50−63.

(14) Eiríksdóttir, E.; Konate, K.; Langel, Ü.; Divita, G.; Deshayes, S. Secondary Structure of Cell-Penetrating Peptides Controls Membrane Interaction and Insertion. *Biochim. Biophys. Acta, Biomembr.* **2010**, *1798*, 1119−1128.

(15) Vivès, E.; Brodin, P.; Lebleu, B. A Truncated Hiv-1 Tat Protein Basic Domain Rapidly Translocates through the Plasma Membrane and Accumulates in the Cell Nucleus. *J. Biol. Chem.* **1997**, *272*, 16010−16017.

(16) Derossi, D.; Joliot, A. H.; Chassaing, G.; Prochiantz, A. The Third Helix of the Antennapedia Homeodomain Translocates through Biological Membranes. *J. Biol. Chem.* **1994**, *269*, 10444−10450.

(17) Futaki, S. Oligoarginine Vectors for Intracellular Delivery: Design and Cellular-Uptake Mechanisms. *Biopolymers* **2006**, *84*, 241−249.

(18) Futaki, S.; Suzuki, T.; Ohashi, W.; Yagami, T.; Tanaka, S.; Ueda, K.; Sugiura, Y. Arginine-Rich Peptides: An Abundant Source of Membrane-Permeable Peptides Having Potential as Carriers for Intracellular Protein Delivery. *J. Biol. Chem.* **2001**, *276*, 5836−5840.

(19) Agrawal, P.; Bhalla, S.; Usmani, S. S.; Singh, S.; Chaudhary, K.; Raghava, G. P. S.; Gautam, A. Cppsite 2.0: A Repository of Experimentally Validated Cell-Penetrating Peptides. *Nucleic Acids Res.* **2016**, *44*, D1098−D1103.

(20) Wang, F.; Wang, Y.; Zhang, X.; Zhang, W.; Guo, S.; Jin, F. Recent Progress of Cell-Penetrating Peptides as New Carriers for Intracellular Cargo Delivery. *J. Controlled Release* **2014**, *174*, 126−136.

(21) Stanzl, E. G.; Trantow, B. M.; Vargas, J. R.; Wender, P. A. Fifteen Years of Cell-Penetrating, Guanidinium-Rich Molecular Transporters: Basic Science, Research Tools, and Clinical Applications. *Acc. Chem. Res.* **2013**, *46*, 2944−2954.

(22) Richard, J. P.; Melikov, K.; Brooks, H.; Prevot, P.; Lebleu, B.; Chernomordik, L. V. Cellular Uptake of Unconjugated Tat Peptide

DOI: 10.1021/acscentsci.8b00446
ACS Cent. Sci. 2018, 4, 1379−1393

Involves Clathrin-Dependent Endocytosis and Heparan Sulfate Receptors. *J. Biol. Chem.* **2005**, *280*, 15300−15306.
(23) Richard, J. P.; Melikov, K.; Vives, E.; Ramos, C.; Verbeure, B.; Gait, M. J.; Chernomordik, L. V.; Lebleu, B. Cell-Penetrating Peptides. A Reevaluation of the Mechanism of Cellular Uptake. *J. Biol. Chem.* **2003**, *278*, 585−590.
(24) Drin, G.; Cottin, S.; Blanc, E.; Rees, A. R.; Temsamani, J. Studies on the Internalization Mechanism of Cationic Cell-Penetrating Peptides. *J. Biol. Chem.* **2003**, *278*, 31192−31201.
(25) Duchardt, F.; Fotin-Mleczek, M.; Schwarz, H.; Fischer, R.; Brock, R. A Comprehensive Model for the Cellular Uptake of Cationic Cell-Penetrating Peptides. *Traffic* **2007**, *8*, 848−866.
(26) Erazo-Oliveras, A.; Muthukrishnan, N.; Baker, R.; Wang, T. Y.; Pellois, J. P. Improving the Endosomal Escape of Cell-Penetrating Peptides and Their Cargos: Strategies and Challenges. *Pharmaceuticals* **2012**, *5*, 1177−1209.
(27) El-Sayed, A.; Futaki, S.; Harashima, H. Delivery of Macromolecules Using Arginine-Rich Cell-Penetrating Peptides: Ways to Overcome Endosomal Entrapment. *AAPS J.* **2009**, *11*, 13−22.
(28) Guidotti, G.; Brambilla, L.; Rossi, D. Cell-Penetrating Peptides: From Basic Research to Clinics. *Trends Pharmacol. Sci.* **2017**, *38* (4), 406−424.
(29) Mix, K. A.; Lomax, J. E.; Raines, R. T. Cytosolic Delivery of Proteins by Bioreversible Esterification. *J. Am. Chem. Soc.* **2017**, *139*, 14396−14398.
(30) Lönn, P.; Kacsinta, A. D.; Cui, X.-S.; Hamil, A. S.; Kaulich, M.; Gogoi, K.; Dowdy, S. F. Enhancing Endosomal Escape for Intracellular Delivery of Macromolecular Biologic Therapeutics. *Sci. Rep.* **2016**, *6*, 32301.
(31) Nagel, Y. A.; Raschle, P. S.; Wennemers, H. Effect of Preorganized Charge-Display on the Cell-Penetrating Properties of Cationic Peptides. *Angew. Chem., Int. Ed.* **2017**, *56*, 122−126.
(32) Mout, R.; Ray, M.; Tay, T.; Sasaki, K.; Yesilbag Tonga, G.; Rotello, V. M. General Strategy for Direct Cytosolic Protein Delivery Via Protein−Nanoparticle Co-Engineering. *ACS Nano* **2017**, *11*, 6416−6421.
(33) Salerno, J. C.; Ngwa, V. M.; Nowak, S. J.; Chrestensen, C. A.; Healey, A. N.; McMurry, J. L. Novel Cell-Penetrating Peptide-Adaptors Effect Intracellular Delivery and Endosomal Escape of Protein Cargos. *J. Cell Sci.* **2016**, *129*, 893−897.
(34) Herce, H. D.; Schumacher, D.; Schneider, A. F. L.; Ludwig, A. K.; Mann, F. A.; Fillies, M.; Kasper, M.-A.; Reinke, S.; Krause, E.; Leonhardt, H.; Cardoso, M. C.; Hackenberger, C. P. R. Cell-Permeable Nanobodies for Targeted Immunolabelling and Antigen Manipulation in Living Cells. *Nat. Chem.* **2017**, *9*, 762−771.
(35) Qian, Z.; LaRochelle, J. R.; Jiang, B.; Lian, W.; Hard, R. L.; Selner, N. G.; Luechapanichkul, R.; Barrios, A. M.; Pei, D. Early Endosomal Escape of a Cyclic Cell-Penetrating Peptide Allows Effective Cytosolic Cargo Delivery. *Biochemistry* **2014**, *53*, 4034−4046.
(36) Erazo-Oliveras, A.; Najjar, K.; Dayani, L.; Wang, T.-Y.; Johnson, G. A.; Pellois, J.-P. Protein Delivery into Live Cells by Incubation with an Endosomolytic Agent. *Nat. Methods* **2014**, *11*, 861−867.
(37) Gaj, T.; Liu, J.; Anderson, K. E.; Sirk, S. J.; Barbas, C. F. Protein Delivery Using Cys2−His2 Zinc-Finger Domains. *ACS Chem. Biol.* **2014**, *9*, 1662−1667.
(38) Appelbaum, J. S.; LaRochelle, J. R.; Smith, B. A.; Balkin, D. M.; Holub, J. M.; Schepartz, A. Arginine Topology Controls Escape of Minimally Cationic Proteins from Early Endosomes to the Cytoplasm. *Chem. Biol.* **2012**, *19*, 819−830.
(39) D'Astolfo, D. S.; Pagliero, R. J.; Pras, A.; Karthaus, W. R.; Clevers, H.; Prasad, V.; Lebbink, R. J.; Rehmann, H.; Geijsen, N. Efficient Intracellular Delivery of Native Proteins. *Cell* **2015**, *161*, 674−690.
(40) Jha, D.; Mishra, R.; Gottschalk, S.; Wiesmüller, K.-H.; Ugurbil, K.; Maier, M. E.; Engelmann, J. Cylop-1: A Novel Cysteine-Rich Cell-Penetrating Peptide for Cytosolic Delivery of Cargoes. *Bioconjugate Chem.* **2011**, *22*, 319−328.
(41) Nischan, N.; Herce, H. D.; Natale, F.; Bohlke, N.; Budisa, N.; Cardoso, M. C.; Hackenberger, C. P. R. Covalent Attachment of Cyclic Tat Peptides to Gfp Results in Protein Delivery into Live Cells with Immediate Bioavailability. *Angew. Chem., Int. Ed.* **2015**, *54*, 1950−1953.
(42) Chang, H.; Lv, J.; Gao, X.; Wang, X.; Wang, H.; Chen, H.; He, X.; Li, L.; Cheng, Y. Rational Design of a Polymer with Robust Efficacy for Intracellular Protein and Peptide Delivery. *Nano Lett.* **2017**, *17*, 1678−1684.
(43) Akishiba, M.; Takeuchi, T.; Kawaguchi, Y.; Sakamoto, K.; Yu, H.-H.; Nakase, I.; Takatani-Nakase, T.; Madani, F.; Gräslund, A.; Futaki, S. Cytosolic Antibody Delivery by Lipid-Sensitive Endosomolytic Peptide. *Nat. Chem.* **2017**, *9*, 751−761.
(44) Herrera Estrada, L. P.; Champion, J. A. Protein Nanoparticles for Therapeutic Protein Delivery. *Biomater. Sci.* **2015**, *3*, 787−799.
(45) Zhao, H.; Lin, Z. Y.; Yildirimer, L.; Dhinakar, A.; Zhao, X.; Wu, J. Polymer-Based Nanoparticles for Protein Delivery: Design, Strategies and Applications. *J. Mater. Chem. B* **2016**, *4*, 4060−4071.
(46) Holub, J. M.; LaRochelle, J. R.; Appelbaum, J. S.; Schepartz, A. Improved Assays for Determining the Cytosolic Access of Peptides, Proteins, and Their Mimetics. *Biochemistry* **2013**, *52*, 9036−9046.
(47) LaRochelle, J. R.; Cobb, G. B.; Steinauer, A.; Rhoades, E.; Schepartz, A. Fluorescence Correlation Spectroscopy Reveals Highly Efficient Cytosolic Delivery of Certain Penta-Arg Proteins and Stapled Peptides. *J. Am. Chem. Soc.* **2015**, *137*, 2536−2541.
(48) Peitz, M.; Pfannkuche, K.; Rajewsky, K.; Edenhofer, F. Ability of the Hydrophobic Fgf and Basic Tat Peptides to Promote Cellular Uptake of Recombinant Cre Recombinase: A Tool for Efficient Genetic Engineering of Mammalian Genomes. *Proc. Natl. Acad. Sci. U. S. A.* **2002**, *99*, 4489−4494.
(49) Zuris, J. A.; Thompson, D. B.; Shu, Y.; Guilinger, J. P.; Bessen, J. L.; Hu, J. H.; Maeder, M. L.; Joung, J. K.; Chen, Z.-Y.; Liu, D. R. Cationic Lipid-Mediated Delivery of Proteins Enables Efficient Protein-Based Genome Editing in Vitro and in Vivo. *Nat. Biotechnol.* **2015**, *33*, 73−80.
(50) Dixon, J. E.; Osman, G.; Morris, G. E.; Markides, H.; Rotherham, M.; Bayoussef, Z.; El Haj, A. J.; Denning, C.; Shakesheff, K. M. Highly Efficient Delivery of Functional Cargoes by the Synergistic Effect of Gag Binding Motifs and Cell-Penetrating Peptides. *Proc. Natl. Acad. Sci. U. S. A.* **2016**, *113*, E291−E299.
(51) Wender, P. A.; Goun, E. A.; Jones, L. R.; Pillow, T. H.; Rothbard, J. B.; Shinde, R.; Contag, C. H. Real-Time Analysis of Uptake and Bioactivatable Cleavage of Luciferin-Transporter Conjugates in Transgenic Reporter Mice. *Proc. Natl. Acad. Sci. U. S. A.* **2007**, *104*, 10340−10345.
(52) Loison, F.; Nizard, P.; Sourisseau, T.; Le Goff, P.; Debure, L.; Le Drean, Y.; Michel, D. A Ubiquitin-Based Assay for the Cytosolic Uptake of Protein Transduction Domains. *Mol. Ther.* **2005**, *11*, 205−214.
(53) Verdurmen, W. P. R.; Mazlami, M.; Plückthun, A. A Quantitative Comparison of Cytosolic Delivery Via Different Protein Uptake Systems. *Sci. Rep.* **2017**, *7*, 13194.
(54) Li, M.; Tao, Y.; Shu, Y.; LaRochelle, J. R.; Steinauer, A.; Thompson, D.; Schepartz, A.; Chen, Z.-Y.; Liu, D. R. Discovery and Characterization of a Peptide That Enhances Endosomal Escape of Delivered Proteins in Vitro and in Vivo. *J. Am. Chem. Soc.* **2015**, *137*, 14084−14093.
(55) Gassmann, M.; Grenacher, B.; Rohde, B.; Vogel, J. Quantifying Western Blots: Pitfalls of Densitometry. *Electrophoresis* **2009**, *30*, 1845−1855.
(56) Cheung, J. C.; Kim Chiaw, P.; Deber, C. M.; Bear, C. E. A Novel Method for Monitoring the Cytosolic Delivery of Peptide Cargo. *J. Controlled Release* **2009**, *137*, 2−7.
(57) Qian, Z.; Dougherty, P. G.; Pei, D. Monitoring the Cytosolic Entry of Cell-Penetrating Peptides Using a Ph-Sensitive Fluorophore. *Chem. Commun.* **2015**, *51*, 2162−2165.
(58) Chao, T.-Y.; Raines, R. T. Fluorogenic Label to Quantify the Cytosolic Delivery of Macromolecules. *Mol. BioSyst.* **2013**, *9*, 339−342.

DOI: 10.1021/acscentsci.8b00446
ACS Cent. Sci. 2018, 4, 1379−1393

(59) Qian, Z.; Liu, T.; Liu, Y.-Y.; Briesewitz, R.; Barrios, A. M.; Jhiang, S. M.; Pei, D. Efficient Delivery of Cyclic Peptides into Mammalian Cells with Short Sequence Motifs. *ACS Chem. Biol.* **2013**, *8*, 423−431.
(60) Milech, N.; Longville, B. A. C.; Cunningham, P. T.; Scobie, M. N.; Bogdawa, H. M.; Winslow, S.; Anastasas, M.; Connor, T.; Ong, F.; Stone, S. R.; Kerfoot, M.; Heinrich, T.; Kroeger, K. M.; Tan, Y.-F.; Hoffmann, K.; Thomas, W. R.; Watt, P. M.; Hopkins, R. M. Gfp-Complementation Assay to Detect Functional Cpp and Protein Delivery into Living Cells. *Sci. Rep.* **2016**, *5*, 18329.
(61) Kim, J.-s.; Choi, D.-K.; Park, S.-w.; Shin, S.-M.; Bae, J.; Kim, D.-M.; Yoo, T. H.; Kim, Y.-S. Quantitative Assessment of Cellular Uptake and Cytosolic Access of Antibody in Living Cells by an Enhanced Split Gfp Complementation Assay. *Biochem. Biophys. Res. Commun.* **2015**, *467*, 771−777.
(62) Peraro, L.; Deprey, K. L.; Moser, M. K.; Zou, Z.; Ball, H. L.; Levine, B.; Kritzer, J. A. Cell Penetration Profiling Using the Chloroalkane Penetration Assay. *J. Am. Chem. Soc.* **2018**, *140*, 11360−11369.
(63) Smith, B. A.; Daniels, D. S.; Coplin, A. E.; Jordan, G. E.; McGregor, L. M.; Schepartz, A. Minimally Cationic Cell-Permeable Miniature Proteins Via α-Helical Arginine Display. *J. Am. Chem. Soc.* **2008**, *130*, 2948−2949.
(64) Kim, S. A.; Heinze, K. G.; Schwille, P. Fluorescence Correlation Spectroscopy in Living Cells. *Nat. Methods* **2007**, *4*, 963−973.
(65) Bacia, K.; Haustein, E.; Schwille, P. Fluorescence Correlation Spectroscopy: Principles and Applications. *Cold Spring Harbor Protocols* **2014**, *2014*, pdb.top081802.
(66) Hess, S. T.; Huang, S.; Heikal, A. A.; Webb, W. W. Biological and Chemical Applications of Fluorescence Correlation Spectroscopy: A Review. *Biochemistry* **2002**, *41*, 697−705.
(67) Keppler, A.; Gendreizig, S.; Gronemeyer, T.; Pick, H.; Vogel, H.; Johnsson, K. A General Method for the Covalent Labeling of Fusion Proteins with Small Molecules in Vivo. *Nat. Biotechnol.* **2003**, *21*, 86−89.
(68) Lam, S. S.; Martell, J. D.; Kamer, K. J.; Deerinck, T. J.; Ellisman, M. H.; Mootha, V. K.; Ting, A. Y. Directed Evolution of Apex2 for Electron Microscopy and Proximity Labeling. *Nat. Methods* **2015**, *12*, 51−54.
(69) Gautier, A.; Juillerat, A.; Heinis, C.; Corrêa, I. R.; Kindermann, M.; Beaufils, F.; Johnsson, K. An Engineered Protein Tag for Multiprotein Labeling in Living Cells. *Chem. Biol.* **2008**, *15*, 128−136.
(70) Los, G. V.; Encell, L. P.; McDougall, M. G.; Hartzell, D. D.; Karassina, N.; Zimprich, C.; Wood, M. G.; Learish, R.; Ohana, R. F.; Urh, M.; Simpson, D.; Mendez, J.; Zimmerman, K.; Otto, P.; Vidugiris, G.; Zhu, J.; Darzins, A.; Klaubert, D. H.; Bulleit, R. F.; Wood, K. V. Halotag: A Novel Protein Labeling Technology for Cell Imaging and Protein Analysis. *ACS Chem. Biol.* **2008**, *3*, 373−382.
(71) Siegel, A. P.; Baird, M. A.; Davidson, M. W.; Day, R. N. Strengths and Weaknesses of Recently Engineered Red Fluorescent Proteins Evaluated in Live Cells Using Fluorescence Correlation Spectroscopy. *Int. J. Mol. Sci.* **2013**, *14*, 20340−20358.
(72) Piatkevich, K. D.; Verkhusha, V. V. Guide to Red Fluorescent Proteins and Biosensors for Flow Cytometry. *Methods Cell Biol.* **2011**, *102*, 431−461.
(73) Keppler, A.; Pick, H.; Arrivoli, C.; Vogel, H.; Johnsson, K. Labeling of Fusion Proteins with Synthetic Fluorophores in Live Cells. *Proc. Natl. Acad. Sci. U. S. A.* **2004**, *101*, 9955−9959.
(74) Mollwitz, B.; Brunk, E.; Schmitt, S.; Pojer, F.; Bannwarth, M.; Schiltz, M.; Rothlisberger, U.; Johnsson, K. Directed Evolution of the Suicide Protein O6-Alkylguanine-DNA Alkyltransferase for Increased Reactivity Results in an Alkylated Protein with Exceptional Stability. *Biochemistry* **2012**, *51*, 986−994.
(75) Wu, Q.; Ploegh, H. L.; Truttmann, M. C. Hepta-Mutant Staphylococcus Aureus Sortase A (SrtA7M) as a Tool for in Vivo Protein Labeling in Caenorhabditis Elegans. *ACS Chem. Biol.* **2017**, *12*, 664−673.
(76) Qian, Z.; Martyna, A.; Hard, R. L.; Wang, J.; Appiah-Kubi, G.; Coss, C.; Phelps, M. A.; Rossman, J. S.; Pei, D. Discovery and Mechanism of Highly Efficient Cyclic Cell-Penetrating Peptides. *Biochemistry* **2016**, *55*, 2601−2612.
(77) Yin, J.; Straight, P. D.; McLoughlin, S. M.; Zhou, Z.; Lin, A. J.; Golan, D. E.; Kelleher, N. L.; Kolter, R.; Walsh, C. T. Genetically Encoded Short Peptide Tag for Versatile Protein Labeling by Sfp Phosphopantetheinyl Transferase. *Proc. Natl. Acad. Sci. U. S. A.* **2005**, *102*, 15815−15820.
(78) Rabideau, A. E.; Liao, X. L.; Akcay, G.; Pentelute, B. L. Translocation of Non-Canonical Polypeptides into Cells Using Protective Antigen. *Sci. Rep.* **2015**, *5*, 11944.
(79) Nakase, I.; Niwa, M.; Takeuchi, T.; Sonomura, K.; Kawabata, N.; Koike, Y.; Takehashi, M.; Tanaka, S.; Ueda, K.; Simpson, J. C.; Jones, A. T.; Sugiura, Y.; Futaki, S. Cellular Uptake of Arginine-Rich Peptides: Roles for Macropinocytosis and Actin Rearrangement. *Mol. Ther.* **2004**, *10*, 1011−1022.
(80) Jones, S. W.; Christison, R.; Bundell, K.; Voyce, C. J.; Brockbank, S. M. V.; Newham, P.; Lindsay, M. A. Characterisation of Cell-Penetrating Peptide-Mediated Peptide Delivery. *Br. J. Pharmacol.* **2005**, *145*, 1093−1102.
(81) Kuhn, T.; Ihalainen, T. O.; Hyvaluoma, J.; Dross, N.; Willman, S. F.; Langowski, J.; Vihinen-Ranta, M.; Timonen, J. Protein Diffusion in Mammalian Cell Cytoplasm. *PLoS One* **2011**, *6*, No. e22962.
(82) Huotari, J.; Helenius, A. Endosome Maturation. *EMBO J.* **2011**, *30*, 3481−3500.
(83) Hung, V.; Udeshi, N. D.; Lam, S. S.; Loh, K. H.; Cox, K. J.; Pedram, K.; Carr, S. A.; Ting, A. Y. Spatially Resolved Proteomic Mapping in Living Cells with the Engineered Peroxidase Apex2. *Nat. Protoc.* **2016**, *11*, 456−475.
(84) Guimaraes, C. P.; Witte, M. D.; Theile, C. S.; Bozkurt, G.; Kundrat, L.; Blom, A. E. M.; Ploegh, H. L. Site-Specific C-Terminal Internal Loop Labeling of Proteins Using Sortase-Mediated Reactions. *Nat. Protoc.* **2013**, *8*, 1787−1799.
(85) Cronican, J. J.; Thompson, D. B.; Beier, K. T.; McNaughton, B. R.; Cepko, C. L.; Liu, D. R. Potent Delivery of Functional Proteins into Mammalian Cells in Vitro and in Vivo Using a Supercharged Protein. *ACS Chem. Biol.* **2010**, *5*, 747−752.
(86) Thompson, D. B.; Villaseñor, R.; Dorr, B. M.; Zerial, M.; Liu, D. R. Cellular Uptake Mechanisms and Endosomal Trafficking of Supercharged Proteins. *Chem. Biol.* **2012**, *19*, 831−843.
(87) Cronican, J. J.; Beier, K. T.; Davis, T. N.; Tseng, J.-C.; Li, W.; Thompson, D. B.; Shih, A. F.; May, E. M.; Cepko, C. L.; Kung, A. L.; Zhou, Q.; Liu, D. R. A Class of Human Proteins That Deliver Functional Proteins into Mammalian Cells In vitro and In vivo. *Chem. Biol.* **2011**, *18*, 833−838.
(88) Andersen, K. A.; Smith, T. P.; Lomax, J. E.; Raines, R. T. Boronic Acid for the Traceless Delivery of Proteins into Cells. *ACS Chem. Biol.* **2016**, *11*, 319−323.
(89) Bruce, V. J.; Lopez-Islas, M.; McNaughton, B. R. Resurfaced Cell-Penetrating Nanobodies: A Potentially General Scaffold for Intracellularly Targeted Protein Discovery. *Protein Sci.* **2016**, *25*, 1129−1137.
(90) Beilhartz, G. L.; Sugiman-Marangos, S. N.; Melnyk, R. A. Repurposing Bacterial Toxins for Intracellular Delivery of Therapeutic Proteins. *Biochem. Pharmacol.* **2017**, *142*, 13−20.
(91) Gibson, D. G.; Young, L.; Chuang, R.-Y.; Venter, J. C.; Hutchison, C. A.; Smith, H. O. Enzymatic Assembly of DNA Molecules up to Several Hundred Kilobases. *Nat. Methods* **2009**, *6*, 343−345.
(92) Nitsche, J. M.; Chang, H.-C.; Weber, P. A.; Nicholson, B. J. A Transient Diffusion Model Yields Unitary Gap Junctional Permeabilities from Images of Cell-to-Cell Fluorescent Dye Transfer between Xenopus Oocytes. *Biophys. J.* **2004**, *86*, 2058−2077.
(93) Weiss, M.; Hashimoto, H.; Nilsson, T. Anomalous Protein Diffusion in Living Cells as Seen by Fluorescence Correlation Spectroscopy. *Biophys. J.* **2003**, *84*, 4043−4052.
(94) Bronstein, I.; Israel, Y.; Kepten, E.; Mai, S.; Shav-Tal, Y.; Barkai, E.; Garini, Y. Transient Anomalous Diffusion of Telomeres in the Nucleus of Mammalian Cells. *Phys. Rev. Lett.* **2009**, *103*, No. 018102, DOI: 10.1103/PhysRevLett.103.018102.

DOI: 10.1021/acscentsci.8b00446
ACS Cent. Sci. 2018, 4, 1379−1393